Stony Brook University

Improving Cardiac Conduction with a Skeletal Muscle Sodium Channel

A Dissertation Presented

by

Jia Lu

To

The Graduate School

In Partial Fulfillment of the

Requirements

for the Degree of

Doctor of Philosophy

in

Physiology and Biophysics

Stony Brook University

December 2008

Stony Brook University

The Graduate School

Jia Lu

We, the dissertation committee for the above candidate for the

Doctor of Philosophy degree, hereby recommend

acceptance of this dissertation.

Ira S. Cohen – Dissertation Advisor
Leading Professor, Physiology and Biophysics, Stony Brook University

Peter R. Brink – Chairperson of Defense
Professor and Chairman, Physiology and Biophysics, Stony Brook University

Emilia Entcheva – Member
Associate Professor, Biomedical Engineering, Stony Brook University

Jianmin Cui – Member
Associate Professor, Biomedical Engineering, Washington University in St. Louis

This dissertation is accepted by the Graduate School.

Lawrence Martin

Dean of the Graduate School

Abstract of the Dissertation

Improving Cardiac Conduction with a Skeletal Muscle Sodium Channel

by

Jia Lu

Doctor of Philosophy

in

Physiology and Biophysics

Stony Brook University

2008

The basic pathology underlying arrhythmias involves malfunction of a number of ion channels which leads to defects of generation and/or propagation of action potentials. Pharmacological treatment usually terminates arrhythmias by making slow conduction fail, while gene and cell therapy aim to remodel ion channel function to improve cardiac conduction. Because the Na^+ channel plays an important role in the upstroke of action potential, increasing Na^+ conductance may speed the propagation of action potential. In this study, we proposed the use of the skeletal muscle Na^+ channel SkM-1 as a more favorable gene than the cardiac isoform SCN5A to enhance conduction velocity in depolarized tissue. Instead of direct delivery of the gene into cardiac tissue by virus as an alternative, we used transfected cell lines as a delivery platform to introduce the Na^+ channels to a cardiac syncytium. Here, we reported that:

1. When these two Na^+ channels were expressed in our delivery cell lines, SkM-1 had a more depolarized inactivation versus voltage curve than SCN5A, a mid point of -53 mV compared with -72 mV in human embryonic kidney (HEK) 293 cells and -59mV compared with -74mV in canine mesenchymal stem cells (cMSCs). We also found that SkM-1 recovered faster from inactivation than SCN5A at both hyperpolarized and depolarized holding potentials. These properties of SkM-1 allow more Na^+ channels to activate at any diastolic membrane potential and faster recovery may also improve conduction.

2. When coupled with SkM-1 expressing cells, cultured adult myocytes showed an increase in the dV/dt_{max} of the action potential in both normal (5.4mM K^+) and depolarized (10.4mM K^+) conditions. This increase was especially significant at -60 and -55 mV. However, expression of SCN5A had no such effect.

3. We also tested the effect of SkM-1 on an *in vitro* cardiac syncytium containing from neonatal ventricular myocytes, and found that coculture of myocytes with HEK293-SkM-1 cells but not HEK293-SCN5A cells significantly increased the conduction velocity of the syncytium under both normal (5.4mM K^+) and depolarized (10.4mM K^+) conditions.

4. Because many tarchyarrhythmias are associated with a re-entrant mechanism, we then set up an *in vitro* re-entry model by high frequency stimulation to test if SkM-1 could also function in an arrhythmic milieu. We found that the SkM-1 coculture has a faster angular velocity of the induced re-entry than the control and SCN5A cultures under both normal and depolarized

conditions, which suggests the potential of SkM-1 to terminate the re-entrant propagation.

In conclusion, these results establish a foundation which supports the hypothesis: **cells carrying non-cardiac Na^+ channel isoforms with a more depolarized inactivation versus voltage curve can improve cardiac excitability and conduction in depolarized tissues**.

Dedicated to my family and my grandfather's 90th birthday.

Table of Contents

List of Figures

List of Tables

Acknowledgements

I am deeply grateful to many people who have dedicated themselves to the work presented in this dissertation. First of all, I would like to give my greatest gratitude and respect to my advisor Dr. Ira Cohen. From his precious guidance, I understand what is doing scientific research. I learned how to face and tackle problems during practical experiments, which can never be learned from any textbook. Ira is not only an intelligent instructor to my study and research, but will always be a wise mentor to my life.

Second, I appreciate Dr. Peter Brink, the chairperson of the committee of my defense. He gave me many insightful instructions to my work from his very unique and precious sight of science. I would like to thank Dr. Emilia Entcheva as well. Without her invaluable instruction and advice, I could not finish the dynamic functional studies in this dissertation. I also want to acknowledge Dr. Cui who comes from Washington University in St. Louis to be my committee member and has attended my defense. He provided me many important comments and suggestions for the proposal and the final dissertation.

Furthermore, I want to thank all the professors in our department who ever taught me. They are all excellent teachers who guide me through the coursework successfully, which provides a solid foundation to my research.

I would like to thank each member, either current or previous, in our laboratory. Everyone contributed to and helped me with this work. Without their cooperation, this dissertation would not be possible.

I want to give special thanks to Dr. Hongzhan Wang in Dr. Brink's laboratory, who helps me with the *double patch clamp* experiments, which was the most challenging part in our research. I also appreciate Chris Gordon for the preparation of adult canine myocytes for me.

Our dynamic functional research was all done in Dr. Entcheva's cardiac cell engineering laboratory, which is an energetic and enjoyable laboratory with a lot of nice people. Particularly, I want to thank Dr. Chiung-yin Chung, Zhiheng Jia, and Dr. Harold Bien who help me to work with their microscopic and macroscopic experimental set ups. I also thank the people in their lab doing the tissue culture to prepare the neonatal myocytes.

Next, I would like to thank Dr. Junyuan Gao in Dr. Richard Mathias's laboratory for teaching me the *patch clamp* technique, which is a fundamental step to electrophysiological research.

I appreciate all staff in Department of Physiology and Biophysics, expecially, the graduate Ph.D. program administrator, Melanie Bonnette, who has been helping me a lot during these years.

Finally, I would like to express my appreciation and love to all my friends and my family members. It is their encouragement and company to support me to walk through this long way of pursuing my Ph.D. degree.

BACKGROUND AND SIGNIFICANCE

1. Cardiac Conduction System (CCS)

The heart is a well-organized organ that autonomically modulates its beating rate during a normal lifetime. It contains an underlying electrical conduction system, which works as a “communication network” for the heart by propagating the rhythmic impulses originated by the sinoatrial node throughout the whole heart and by doing so stimulating the contraction of the myocardium to pump blood to the body.

1.1 Cardiac conduction pathway

The cardiac conduction pathway includes the sinoatrial (SA) node, the atrium, the atrioventricular (AV) node, the Bundle of His and its branches, and finally ventricular muscle (Fig 1). Rhythmic electrical impulses (spontaneous action potentials) arising from the pacemaker cells of the SA node travel rapidly to the atria causing their contraction. The impulse then continues to the AV node. The AV node delays the stimuli before passing them to the bundle of His and then into the peripheral Purkinje fibers and finally to the ventricles. This A-V nodal delay ensures the atria sufficient time to contract and thus helps to fill the ventricles more completely with blood during ventricular relaxation. The signals finally reach the ventricular myocardium leading to contraction and resulting in the cardiac output[1].

1.2 Conduction velocity and its determinants

To maintain a coordinated and efficient contraction of the heart, the conduction pathway is designed with heterogeneous properties[2]. One of the most important manifestations is the regional difference in the conduction velocity (CV) of action potential propagation: CV is higher in the atrial, ventricular and His-Purkinje tissues, but lower in the nodal cells (Table 1). The fast conduction in the His-Purkinje system ensures a nearly synchronous contraction of the ventricles, while the slow conduction in the AV node allows the atrial contraction to maximally fill the ventricles before they contract.

In addition to electrical cell-to-cell coupling (functional gap junctions) which determines the axial resistance along with the myoplasm[3], the conduction velocity depends on the membrane properties that give rise to the conducting electrical event, action potentials (APs). Indeed, cardiac APs vary in different parts of the heart and the different AP characteristics are in large part related to their ion channel activities[4].

For example, in a typical AP of a ventricular myocyte (Fig 2A), there are five phases[4]. Starting from a maximum diastolic potential (phase 4), a cell undergoes a rapid depolarization (phase 0) due to the opening of fast Na channels and a large Na^+ inward current (in ventricle there is also a small contribution of L-type calcium current to the action potential upstroke). Next, the inactivation of Na^+ channels and a net outward K^+ current carried by I_{to1} generates a rapid initial repolarization (phase 1). This is followed by a sustained "plateau" (phase 2) mainly due to inward Ca^{2+} current though L-type Ca^{2+}

channels, and outward K^+ current through the slow delayed rectifier K channels (I_{kr} and I_{ks}). Then the closing of L-type Ca^{2+} channels along with further activation of the delayed rectifiers along with the background inward rectifier K^+ channels, leads to the repolarization of the membrane potential (phase 3). Finally the delayed rectifier K^+ channels close and the inward rectifier K^+ channel maintains the myocyte at the basal maximum diastolic (resting) potential.

Things are quite different in nodal cells which have low conduction velocities (Fig 2B). Although these cells may also express Na^+ channels, relatively positive resting potentials (~60 mV) result in inactivation of these channels. Lacking fast inward Na^+ currents, the membrane of a nodal cell slowly depolarizes during the upstroke of AP caused by Ca^{2+} channels with slower kinetics and smaller currents[4]. The pacemaker potential of the SA nodal cells is determined at least in part by the turn off of the delayed rectifier I_{kr} and the activation of the hypolarization activated current I_f [5].

Thus, the conduction velocity of action potential propagation is strongly influenced by their excitatory inward current, which determines the rate of rise of the upstrokes (phase 0) of the action potential. Normally, Na^+ channels endow values from 200 to 900 V/sec to the maximum rate of rise (dV/dt_{max}) of the action potentials in the atrial, ventricular and His-Purkinje cells[4]. By contrast, the values of dV/dt_{max} are on order of 5-50 V/sec in the nodal cells because of the much smaller conductance to L-type calcium channels and their much slower kinetics of activation[4].

2. Conduction Disorders and Arrhythmia

Since the heart is a sequential conducting network, any malfunction in the pathway may cause conduction disturbance and arrhythmia. Arrhythmias can originate from a number of cardiac disorders, such as coronary artery disease, heart valve disease, myocarditis, and acute myocardial infarction[6, 7]. They can also result from genetic mutations of the ion channels that open and close during the action potential[8, 9]. The basic pathology underlying arrhythmias relates to abnormalities in the generation or/and propagation of the impulse[10].

2.1 Types of cardiac arrhythmia and their pathology

Abnormal cardiac rhythms can be classified into two types: bradyarrhythmias with excessively slow heart rhythms and tachyarrhythmias with excessively rapid heart rhythms[11].

The bradyarrhythmias can arise from dysfunction of either automaticity (the generation of pacemaker activity) or conduction. Decreased intrinsic pacemaker activity of the SA node underlies some causes of slow heart rates. The SA node dysfunction may result from the damage due to ischemia or other diseases. The other major mechanism of the bradyarrhythmias is known as heart block, usually within the AV node or the His-Purkinje system. It occurs as a result of inflammation and/or scarring of the conducting tissue, some other aging associated disorders or genetic diseases.

The tachyarrhythmias also result from abnormalities of impulse formation and conduction. Enhanced normal automaticity of the SA node and abnormal

automaticity of depolarized atrial, AV, and Purkinje fibers can accelerate the heart rhythm. More commonly, a reentrant propagation mechanism called *re-entry*[12] leads to tachyarrhythmia, such as atrial fibrillation and ventricular tachycardia and fibrillation.

Re-entry often refers to a circular impulse propagation as shown in Fig 3. Pathway A with slower conduction and a shorter refractory period and Pathway B with normal conduction and a longer refractory period connect at 1. In the first case (Fig 3I), an impulse travels through both ways but slowly in A. So the propagation is blocked at 2 which is refractory after conduction through B, which gives a normal beat. In the second situation (Fig 3II), a premature impulse is blocked at 3 in Pathway B. The signal proceeds through A and generates a beat. If the conduction through A is slow enough (Fig 3III) then the propagation reaches B after the tissue has been recovered from refractoriness. The impulse may reenter into A and continue to conduct in circles. So, the occurrence of re-entry requires several conditions: 1) abnormalities of conduction in two or more interconnected pathways; 2) unidirectional conduction block in one pathway; 3) slow enough conduction in another direction or pathway to ensure recovery of excitability in the originally refractory region to form a closed loop. Sustained circulation of the impulse then results in a fast heart rate leading to tachyarrhythmia. Re-entry can happen either globally, such as AV nodal re-entry between atria and ventricles, or in small local areas. Multiple reentrant circuits in the heart may lead to ventricular fibrillation and sudden death. Because most

tachyarrhythmias are associated with this mechanism, re-entry is a good model to study these diseases.

2.2 Underlying ion channel dysfunction in conduction abnormalities

To develop effective therapies for arrhythmia, we should understand its molecular and cellular origins. Most often its origin is uncertain, it can be either acquired or inherited, and the associated conduction problems can be related to changes in the fundamental properties of ion channels[8,9]. One such example is drug-induced long QT syndrome which is related to block of HERG channels by a variety of pharmacologic agents[13,14]. The HERG gene comprises the alpha subunit of the I_{kr} channel which contributes to the repolarization of the action potentials. One of the inherited forms of this syndrome may result from mutations in the subunit of HERG channel[15]. While others result from mutations in other K^+ channel subunits which lead to loss of function or in the cardiac Na^+ channels where gain of function giving increased persistent inward Na^+ current leads to a longer action potential[16,17].

Because of the important role that the Na^+ current plays in cardiac conduction, here we now consider the role of the Na^+ channel in more detail in abnormalities related to disturbances of conduction.

Voltage-gated Na^+ channels are responsible for the rapid upstroke phase of action potentials. The α subunit of human cardiac channel is a 2016 amino acid protein encoded by the *SCN5A* gene[18]. Although there are accessory β subunits, the α subunit forms the channel pore by four repeating domains each

of which has 6 transmembrane regions (S1 to S6) (Fig 4). The four S4 regions comprise the voltage sensor and determine both opening and inactivation of the channel. In the Hodgkin and Huxley formalism for gating Na^+ channels[19], depolarization of the membrane rapidly activates the “m gates” to open the channels and allow inward currents to pass through. On the other hand, depolarization also more slowly inactivates the “h gates” which close the channels and maintain a refractory state. Repolarization of the membrane, at the end of the action potential, brings the channels back to their resting activatable state (Fig 5). Therefore, the gating properties of Na^+ channels directly determine the Na^+ conductance activated during the action potential and in so doing influence the conduction velocity or indeed its basic ability to conduct.

Mutations in the SCN5A gene may lead to arrhythmia either by loss-of-function or gain-of-function (Table 2). Loss-of-function mutations result in non-functional channel proteins or rapid inactivation of the channel, which reduce the availability of Na^+ current to generate the upstroke of the AP thus slowing conduction. As stated above, gain-of-function mutations slow inactivation or reopen the channel during the plateau of the AP leading to a prolonged AP duration and long QT interval in the ECG.

Furthermore, in the border zone of cells surviving myocardial infarction there is a membrane depolarization[20] which indirectly results in a reduction of Na^+ current by inactivating these channels. Besides the membrane depolarization there is also a negative shift in the voltage dependence of steady-

state Na^+ channel availability further compromising the speed at which the damaged ischemic myocytes conduct the AP[21].

Other ion channels, as well as the Na^+ channel, largely remodel in cardiac conduction abnormalities[22,23]. Therefore, to restore normal rhythm and conduction, these ion channels are potential therapeutic targets for antiarrhythmic treatment.

3. Cell and Gene Therapy for Conduction Disorders

Undetected arrhythmias may contribute to more than 300,000 sudden deaths each year in the United States[24], and there are an increasing emergency department visits and hospital admissions for atrial fibrillation[25]. However current antiarrhythmic therapies are relatively imperfect and may have life threatening side effects.

3.1 Current therapies for conduction disorders

Existing treatments include antiarrhythmic drugs, radiofrequency or surgical ablation, and implantation of pacemaker devices[26].

Pharmacotherapy aiming to decrease conduction velocity has been used as a standard treatment for arrhythmias. There are four classes of antiarrhythmic drugs[27]: 1) Na channel blockers, which slow the depolarization of APs and reduce conduction velocity converting unidirectional block to bidirectional block and thus terminating tachyarrhythmias caused by reentry; 2) β_1- adrenoceptors blockers, which inhibit sympathetic effects and in so doing decrease automaticity,

slow conduction and prolong refractoriness for sinus tachycardia, AV node reentry, etc; 3) K^+ channel blockers, which delay the repolarization of the AP and prolong the effective refractory period to abolish excitability in reentrant tachyarrhythmia; 4) Ca^{2+} channel blockers, which inhibit the Ca^{2+} dependent AP in slowly conducting tissue (SA and AV nodes) to reduce automaticity and slow conduction for supraventricular tachycardia.

The major problem of drug therapy is that these same drugs may induce another arrhythmia, some of which may even be lethal[28]. For example, Na^+ channel blockers may totally abolish the conduction that had resulted in reentry, but they may also affect healthy tissues to reduce the conduction velocity and induce reentry. Treatment with β1 receptor blockers or Ca^{2+} channel blockers may lead to AV node block.

In addition, surgical procedures and devices are employed as antiarrhythmic treatments[29,30]. Radiofrequency or surgical ablation helps to destroy the source of the abnormal rhythm, usually for atrial flutter or AV node reentry. For more serious cases, DC cardioversion-defibrillation is used to terminate ventricular tachyarrhythmia and restore sinus rhythm. Implantation of a pacemaker device is required for patients with symptomatic SA node dysfunction or high-grade AV node block. Disadvantages of these invasive approaches include not only the painful procedure itself but also some potential complications, such as bleeding, infection, or device migration. Environmental interference like cell phones or MRIs may also cause pacemaker malfunction[31].

Thus, due to the limitations of these existing treatments, safer and more effective therapeutic approaches need to be developed.

3.2 Gene and cell therapy

Gene therapy

In 1990, gene therapy was employed for the first time for therapy of a patient with severe combined immunodeficiency (SCID)[32]. Since that time gene therapy has been widely investigated for many diseases, including cardiac arrhythmias. Nevertheless although proof of principle has been demonstrated for this therapeutic strategy it is still in its infancy.

Like other antiarrhythmic treatments, gene therapy aims to restore more normal cardiac function by altering the activities of ion channels. An early study reported that overexpression of the inhibitory G protein $G\alpha_{i2}$ in the AV node resulted in reduction of heart rate in an atiral fibrillation animal model[33]. More recently, our group has used the HCN2 gene (a member of the HCN pacemaker gene family) delivered to dog atria or the ventricular conducting system and generated a biological rhythm initiating from the site of injection[34]. These studies initiated an approach using the pacemaker current I_f to generate biological pacemakers.

Compared with drug therapies, the advantages of gene therapy include 1) target local diseased tissue instead of a global effect; 2) introducing favorable genes which can improve conduction velocity other than slow it down.

Stem cell therapy

However viral delivery systems can cause inflammation and also have either a limited period of expression (adenoviruses) or the potential for neoplasia (retroviruses). On the other hand, stem cells represent another novel treatment for heart disease. There have been encouraging results suggesting that delivery of bone marrow derived stem cells can induce cardiac repair after myocardial infarction[35,36]. Considering the limitations of viral gene therapy, our group has used mesenchymal stem cells as a delivery platform for cell therapy.

It is well documented that, stem cells are able to self replicate and to differentiate into many cell types. Mesenchymal stem cells (MSCs) are a small population of cells residing in adult bone marrow, about 10 times less abundant than hematopoietic stem cells (HSCs) but easier to isolate[37]. MSCs not only play important roles in HSC differentiation, they can also give rise to many mesodermal lineages, such as cartilage, bone and fat[38]. Extensive subcultivation can expand MSCs without differentiation but retaining their multipotency[39].

Our group has identified that the mesenchymal stem cells contain the building blocks of gap junctions (connexins) and so are able to form functional gap junctions with cardiac myocytes[40] (Fig 6). They are also thought to be immunopriviledged leading to the possibility of an allogenic therapy[41,42,43]. In 2004 our group took human mesenchymal stem cells (hMSCs) transfected with the mouse HCN2 gene, and implanted them into the canine left ventricle. An on demand biological pacemaker was generated which has since been demonstrated to last at least six weeks *in vivo*[44].

Hence, MSCs can be genetically modified and function as a gene delivery system, providing a new therapeutic approach for cardiac arrhythmia.

INTRODUCTION AND SCOPE OF RESEARCH

1. Targeting Conduction via Na^+ Channels and its Significance

The research of this dissertation is to explore a gene and cell therapy which can restore normal function for cardiac conduction disorders which result in arrhythmia. Abnormalities of cardiac conduction result from malfunctions of membrane ion channels which influence action potential (AP) parameters and/or gap junction channels which influence axial resistance. These changes affect propagation velocity. As discussed in **Background and Significance**, antiarrhythmic pharmacotherapy usually inhibits target ion channels to block conduction or increase refractoriness to terminate reentrant arrhythmias. This might be proarrhythmic for normal tissues because slow conduction is involved in the genesis of reentry. Given the promise of gene and cell therapy and the known molecular correlates of the sodium channels, it is worth considering whether an opposite approach to improve conduction to prevent reentrant tachyarrythmias might be feasible. In addition, this approach might benefit slow conduction disorders, such as AV node block. Our goal is to improve conduction of the depolarized tissue so that it propagates too fast to allow reentry. Thus, the experimental approach of this study was designed to introduce a Na^+ channel which has favorable properties to enhance the upstroke of the AP providing more local circuit current to speed conduction, especially in depolarized conditions.

As stated above, the diseased heart following myocardial infarction is associated with depolarized myocytes which generate arrhythmias. According to the Hodgkin & Huxley formalism of the voltage gated Na^+ channel, the h gate

remains open at normal resting potentials but is inactivated at a depolarized resting potential leading to little availability of Na^+ current for generation of the action potential upstroke. In this case, more native cardiac sodium channel expression would have limited advantages (Fig 7B). Compared with the cardiac isoform, the skeletal muscle Na^+ channel has at least a 10 mV more depolarized midpoint of inactivation (Fig 7A) [45,46]. This difference may allow more skeletal Na^+ channels to have their h gates open during diastole so that more Na^+ current is available at a depolarized resting state (Fig 7C). Thus, the central hypothesis of our work is that "non-cardiac Na^+ channel isoforms with a more depolarized inactivation versus voltage curve should function better to improve conduction in depolarized tissues". Here we selected the skeletal muscle Na^+ channel (SkM-1) gene as our molecular candidate.

Our group has successfully introduced HCN2, a pacemaker channel gene, into the *in vivo* canine myocardium using human mesenchymal stem cells (HMSCs) as a delivery platform[40,44]. These studies suggest that cell based gene delivery is a feasible approach. In this study, cell lines which can be transfected with the gene of interest and electrically couple with cardiac myocytes by forming gap junctions were selected to serve as our gene delivery systems to introduce Na^+ channels to myocytes.

2. Specific Aims:

To identify its antiarrhythmic potential, we studied cell lines expressing SkM-1 *in vitro* and tested the hypothesis: **delivery of SkM-1, a Na^+ channel with**

a depolarized inactivation curve via a cell line which can electrically couple with myocytes through gap junctions, may improve cardiac excitability and conduction to prevent arrhythmia.

Four aims were achieved to test this hypothesis:

Aim 1: To set up cell lines expressing SkM-1 or SCN5A and characterize their biophysical properties.

Two cell lines expressing connexin43 were selected to use as delivery systems for further experiments. Human embryonic kidney (HEK293) cells were used for *in vitro* tests because of easier handling. Canine or human mesenchymal stem cells (MSCs) were considered as a delivery platform for future *in vivo* studies. These cell lines were either stably or transiently transfected with constructs encoding SkM-1 or SCN5A genes. Biophysical properties, including kinetics of activation, inactivation and recovery from inactivation of these two Na^+ channels were identified using the whole cell patch clamp technique.

Aim 2: To compare the effects of SkM-1 and SCN5A on the maximal action potential (AP) rate of rise (dV/dt_{max}) of myocytes coupled to Na^+ channel expressing cells.

To set up a primary cell-to-cell gene delivery model, adult canine ventricular myocytes were isolated and cocultured with HEK293 cells in M199 medium in tissue culture dishes. Within 48 to 72 hr, double patch clamp was

applied to myocyte-HEK293 cell pairs to record the electrical coupling between the two cells. Current clamp was used to generate and record action potentials in the myocytes to test whether dV/dt_{max} of the AP could be increased by SkM-1 current from the HEK293-SkM-1 cell which passes through gap junctions in both normal (5.4 mM K) and depolarized (10.4 mM K) conditions. We compared the AP upstrokes of the myocyte-HEK293-SkM-1 cell pairs with myocytes only, myocyte-HEK293 cell pairs and myocyte-HEK293-SCN5A cell pairs.

Aim 3: To test the effects of SkM-1 and SCN5A on the conduction velocity of action potential propagation in a cell culture model.

We set up an *in vitro* cardiac syncytium to test the effect of introducing Na^+ channels on conduction. Rat neonatal myocytes and HEK293 cells were cocultured on rectangular poly-dimethylsiloxane (PDMS) scaffolds in M199 medium. Cells were cultured for 5 to 6 days allowing them to make gap junctions. In the action potential propagation experiments, one electrode was placed on one side of the scaffold to give stimuli of increasing frequencies. Propagated APs in the cells on the other side of the scaffold was measured in a microscopic system using a voltage sensitive dye as fluorescence changes. Fluorescence signals were recorded with a phtomultiplier tube (PMT) and data acquisition was processed with computer software IONOPTIX. Conduction velocity was measured and calculated to test whether expression of the SkM-1 current in the myocyte and HEK293-SkM-1 coculture could improve propagation under both normal and depolarized conditions. We compared the conduction velocities of

SkM-1 culture with myocytes only, myocytes cocultured with non-transfected HEK293 cells and myocyte-HEK293-SCN5A culture.

Aim 4: To test whether expressing SkM-1 can prevent arrhythmia (re-entry).

Re-entry was artificially generated in the *in vitro* model of cocultured rat neonatal myocytes and HEK293 cells by making a small void in the center of the culture dish. Spontaneous spiral AP propagation around the hole was introduced by stimulating the culture at high frequencies with a point electrode. The action potential propagation was measured using a calcium sensitive dye in a macroscopic optical mapping system and raw data were analyzed by Matlab software to generate phase movies. Angular velocities of the reentrant propagations were measured under both normal and depolarized conditions to test whether expression of SkM-1 currents in HEK293-SkM-1 cells can speed conduction and possibly prevent reentry. We compared the effects of SkM-1 in this re-entry model with SCN5A.

MATERIALS AND METHODS

Unless otherwise indicated, all chemicals were from Sigma Chemical Co., St Louis, MO.

Plasmid Construction

The rat SkM-1 insert was released from pμI-2-SkM-1 (kindly provided by Dr. Gail Mandel, SUNY, Stony Brook) and subcloned into a mammalian expression vector pIRES2-EGFP (BD Bioscience Clontech, Mountain View, CA) at the EcoR I site.

Human SCN5A-pcDNA3.1 was a kind gift from Dr. Robert Kass, Columbia University). The insert was excised using Hind III and Xba I restriction enzymes, blunt ended, and subcloned into the Sma I site of pIRES2-EGFP.

Orientation and sequences were verified by antomated sequencing.

Cell Culture

Culture of HEK293 cells

HEK293 cells (ATCC, Manassas, VA) were maintained in DMEM (Dulbecco's Modified Eagle's Medium, GIBCO Invitrogen, Carlsbad, CA) supplemented with 10% FBS (fetal bovine serum, Sigma-Aldrich, St Louis MO) and 1% penicillin-streptomycin (Sigma) at 37℃ in a humidified atmosphere incubator with 5% CO_2 and 95% air.

Isolation and characterization of cMSCs

Canine mesenchymal stem cells were isolated from bone marrow of adult dogs. Basically, 4 ml canine bone marrow aspirate, taken from the iliac crest of one year old dog of either sex, were diluted 1:1 with Dulbecco's phosphate-buffer saline (DPBS, GIBCO Invitrogen) containing 750 units heparin, and centrifuged at 900 g for 10 minutes at room temperature. The washed cells were resuspended in DPBS to a final volume of 4 ml and layered over an equal volume of 1.073 g/ml Ficoll-Paque Plus solution (Amersham Biosciences, Pittsburgh, PA). After centrifugation at 900 g for 30 minutes, the mononuclear cells were recovered from the gradient interface and washed with DPBS twice. The bone marrow cells were suspended in DMEM containing 1g/ml of glucose (GIBCO Invitrgen) supplemented with 10% FBS, 100U/ml penicilline, 100 μg/ml streptomycin, and 25 μg/ml amphotericin B. All cells were plated in 10 ml of medium in a 100mm dish at a density of 10^6 mononuclear cells/ cm^2. The cultures were maintained at 37℃ in 5% CO_2 and 95% air with an initial medium for 48 hours, and then medium was changed every 3 to 4 days. Cell colonies with spindle-like morphology were transferred to 12 well plates 7 days after initial plating. After confluence the cells were harvested with 0.25% trypsin-EDTA, and replated in 60mm dishes.

The isolated cells were characterized at passages 2 to 4 by flow cytometirc analysis of specific surface antigens. 5×10^5 cells were harvested from dishes and stained for 30 minutes at room temperature with fluorescein isothiocyanate- (FITC) conjugated rat anti-canine CD44 and phycoerythrin-(PE)

conjugated mouse anti-canine CD34 in 100 μl washing buffer (PBS with 1% sodium azide and 2% BSA). CD44 is a matrix receptor and CD34 is a hematopoietic lineage marker. The stained cells were washed with 2 ml wash buffer twice and then resuspended in 0.5 ml of fix buffer (1% paraformaldehyde, 0.1% sodium azide). The labeled cells were analyzed on FACScan (Becton-Dickinson) by collecting 10,000 events with the cell Quest software program (Becton-Dickinson). About 93.9% of the cells were CD44 positive and 6.1% of the cells were CD34 positive, suggesting a significant majority of the isolated cells were mesenchymal stem cells.

Transfection

Stably transfection of HEK293 cells

HEK293 cells were transfected with the construct DNA using Lipofectamine™ 2000 (from Invitrogen) as directed, about 4 μg DNA for cells of a 35mm culture dish (Falcon BD, San Jose, CA) at 90 to 95% confluency. EGFP expression was examined on the next day. 48 hours after transfection, 500 μg/ml Geneticin (GIBCO Invitrogen) was applied to select the stably transfected cells. The stable cell line then underwent flow cytometry (at the USB Research Flow Cytometry Core Facility, SUNY Stony Brook) to further select GFP-positive cells. Briefly, cells were collected by trypsinization with 0.25% trypsin-EDTA. After centrifugation at 1000 rpm for 4 minutes, cells were resuspended by serum-free DMEM at a concentration of 5 to 10×10^6 cells/ ml. The suspension was then analyzed on FACSan (Becton-Dickinson) by collecting 10,000 events with the

cell Quest software program (Becton-Dickinson) using high-purity sorting. The selected cells with high GFP fluorescence were then maintained in Geneticin (500 μg/ml) containing culture medium at 37℃ in a humidified atmosphere incubator with 5% CO_2 and 95% air.

Transfection of cMSCs

cMSCs were transfected by electroporation using nucleofector technology (Amaxa Lonza, Gaithersburg, MD) as directed. Briefly, cells of a confluent 100 mm tissue culture dish (Falcon BD) (around 1×10^6 cells) were trypsinized by 0.25% trypsin-EDTA (GIBCO Invitrogen) and collected by centrifugation for 4 min at 1000 rpm. Cells were then re-suspended in 100 μl nucleofector solution with 4 μg DNA construct and placed into a nucleofection cuvette. The cuvette was then inserted into Nucleofector Device I and electroporation program U-23 was performed for high transfection efficiency. The cell suspension was finally transferred back to a tissue culture dish and incubated at normal culture conditions. Expression of EGFP and Na^+ currents could be examined 24 to 48 hours after transfection.

Imaging

Images of HEK293-SkM-1 and cMSC-SkM-1 cells were taken and analyzed by an inverted microscope (Olympus IX51, Melville, NY) connected to camera (Olympus DP70) using a DPController software (Olympus).

Whole Cell Patch Clamp Experiments

Patch clamp electrodes

Electrodes were made from patch clamp glass capillaries #PG10150-4 (OD/ID: 1.5 mm/0.75 mm; World Precision Instruments Inc., Sarasota, FL). Two identical patch clamp electrodes were made from a capillary with a P-87 Flaming/Brown micropipette puller (Sutter Instrument Company, Novato, CA) using a programmed multi-step procedure. After filling with electrode solution, the resistances of the electrodes were between 3 to 4 MΩ, identified by computer software pCLAMP 8.2 (Axon instruments Inc.).

To fill the electrodes, we followed two steps: first, we connected the electrodes to a syringe and dipped the tip of the electrode into the electrode solution and applied a negative pressure via suction of the syringe at the other end of the electrode for 5 to 10 seconds, so that the tips were filled. The second step was to backfill about 2/3 of the electrodes with the electrode solution by a syringe with a 0.2 μm filter (Acrodisc, Pall Corporation, Ann Arbor, MI).

Perfusion system and working platform

The perfusion system contains 8 plastic reservoirs, a flow controller, a chamber and vacuum system. The plastic reservoirs were placed approximately 1.5 feet above the chamber so that the perfusion solution could be driven into the chamber by gravity. Different perfusion solutions could be exchanged between reservoirs by a flow controller (cFlow, Cell MicroControls, Norfolk, VA).

The recording chamber was mounted on an inverted microscope (Olympus CK40, Japan) with. GFP-positive cells were viewed through a 40× long working distance objective lenses (Olympus, Japan) and underwent patch clamp.

The whole-cell patch clamp setup

Whole cell patch clamp was used to measure the membrane current in single cells. The set up included an electrode holder (Model EH-07, E.W Wringt, Guilfor, CT) with a AgCl coated silver filament connected to an electrode head stage (CV4, Axon instruments Inc., Burlingame, CA) mounted on the microscope, another AgCl coated wire placed in the chamber as a ground, a micromanipulator (NARISHIGE CO., Tokyo, Japan) to adjust the position of the electrode. The electrode head stage was connected to a signal amplifier (Model Axopatch-1B, Axon Instruments Inc.). Voltage and current signals was recorded by the amplifier and digitized through a digitizer (Model DIGIDATA 1320A, Axon Instruments) and finally transferred to a personal computer. Data acquisition and analysis were performed by the computer using CLAMPEX 9.2 and CLAMFIT 9.2 softwares (Axon instruments), respectively.

The perfusion system, microscope, electrode head stage, and micromanipulator were supported by a vibration isolated air table (Newport research corporation, Valley, CA) to eliminate the vibration from the building during experiments. In addition, a Faraday cage was used to cover the whole working platform to minimize the radiated electromagnetic interference.

Solutions

Normal Tyrode's solution contained (in mM): NaCl 137.7, KCl 5.4, NaOH 2.3, $CaCl_2$ 1.8, $MgCl_2$ 1, Glucose 10, and HEPES 10 (pH adjusted to 7.4 with NaOH).

Low Na^+ Tyrode's solution contained (in mM): NaCl 15, TEACl 122.7, KCl 5.4, NaOH 2.3, $CaCl_2$ 1.8, $MgCl_2$ 1, Glucose 10, and HEPES 10 (pH adjusted to 7.4 with NaOH).

The Electrode solution was filled with (in mM): KCl 50, K-aspartic acid 80, $MgCl_2$ 1, EGTA 10, HEPES 10 and Na_2-ATP_3 (pH adjusted to 7.2 with KOH).

Antibodies

Anti-connexin43 developed in rabbit (Sigma) corresponding to a C-terminal segment of human Cx43 and mouse anti-human Cx45 monoclonal antibody (Chemicon International Inc., Temecula, CA) were used for Western blot. For SkM-1, we used rabbit anit-Pan Na_v (Alomone Labs, Jerusalem, Israel) which recognized a highly homologous loop between III and IV domains of all isoforms of voltage-gated Na^+ channels.

Generation of Canine Ventricular Myocyte and HEK293 Cell Pairs

Preparation of single canine ventricular myocytes

Adult mongrel dogs of either sex weighing 18-22 kg were euthanized by intravenous injection of sodium pentobarbitone (80mg/kg body weight) and the heart removed. Canine ventricular cells were isolated using a modified

Langendorf procedure by perfusing a wedge of left ventricle through a coronary artery with 0.5mg/ml collagenase (Type 2, Worthington, Lakewood, NJ) and 0.08 mg/ml protease (Type XVI, Sigma) for 9 to 11 minutes followed by tissue mincing[47]. Isolated myocytes were stored in Kraft-Brühe (KB) solution at room temperature before coculture with HEK293 cells.

KB solution contains (in mM): KCl, 83; K_2HPO_4, 30; $MgSO_4$, 5; Na-Pyruvic Acid, 5; β-OH-Butyric Acid, 5; Creatine, 5; Taurine, 20; Glucose, 10; EGTA, 0.5; KOH, 2; and Na_2-ATP, 5. The pH was adjusted to 7.2 with KOH.

Coculture of myocytes and HEK293 cells

The cardiomyocytes in KB solution were plated onto mouse laminin (10 μg/ml, Invitrogen) coated coverslips and incubated in a 37℃, 5% CO_2/95% air incubator for 1 hour for attachment and the solution was then replaced by Medium 199 supplemented with 10% FBS, 1% penicillin/streptomycin and 50 μg/ml Gentamicin (Invitrogen). HEK293 cells were typsinized by 0.25% trypsin-EDTA (Gibco Invitrogen) and then collected by centrifugation at 1000 rpm for 4 minutes. The cell pellet was re-suspended in supplemented M199 medium and distributed into the myocyte culture. The cocultures were incubated at 37℃ in a humidified atmosphere with 5% CO_2. Dual patch clamp experiments were performed 48 to 72 hours after plating.

Dual Patch Clamp Experiments

The patch clamp set up

The whole set up included an experimental chamber, a perfusion system, an inverted microscope (Nikon, Japan), an air table (VIBRAPLANE, Boston, MA) filled by a compressed air tank, two electrode head stages adjusted by micromanipulators, two amplifiers (Axopatch 1-D) and a digitizer (DIGIDATA 1322A) connected to a personal computer. When clamping cell pairs, signals from two electrodes, channel 0 and channel 1 were recorded by the amplifiers, digitalized by the digitizer and then transferred into the computer. Data were acquired and analyzed by CLAMPEX 9.0 and CLAMFIT 9.0 software, respectively. The microscope was also connected to a digital 12 bit CCD camera (PixelFly, The Cooke Corp., Romulus, MI) to record the image of the cell pairs using CamWare software in the computer.

Electrodes and solutions

Electrodes with a resistance of 3 to 4 MΩ as in single whole cell patch clamp were used in dual patch clamp.

Normal K^+ Tyrode's solution contained (in mM): NaCl 137.7, KCl 5.4, NaOH 2.3, $CaCl_2$ 1.8, $MgCl_2$ 1, Glucose 10, and HEPES 10 (pH adjusted to 7.4 with NaOH).

High K^+ (10.4 mM) Tyrode's solution contained (in mM): NaCl 132.7, KCl 10.4, NaOH 2.3, $CaCl_2$ 1.8, $MgCl_2$ 1, Glucose 10, and HEPES 10 (pH adjusted to 7.4 with NaOH).

The electrode pipettes were filled with solution containing (in mM): KCl 50, K-aspartic acid 80, $MgCl_2$ 1, EGTA 10, HEPES 10 and Na_2-ATP_3 (pH adjusted to 7.2 with KOH).

Generation of the Cardiac Syncytium

Preparation of neonatal rat ventricular myocytes

Neonatal rat cardiac myocytes were isolated as previously described[48]. Briefly, neonatal Sprague-Dawley rats were sacrificed three days after birth. Cardiac tissue from the ventricles was excised from their chests and washed free of blood. The tissue was then cut into small pieces and enzymatically digested with trypsin (1mg/ml, 4℃, USB, Cleveland, OH), then collagenase (1mg/ml, 37℃, Worthington, Lakewood, NJ) the next morning. The cardiac fibroblasts were removed by ninety minutes of preplating. The isolated myocytes were then ready to be plated.

Coculture of neonatal myocytes with HEK293 cells

Neonatal ventricular myocytes were plated at high densities (4×10^5 cells/cm^2 for the control myocyte group and 3.5×10^5 cells/cm^2 for the coculture groups) onto fibronectin-coated poldimethylsiloxane (PDMS, Sylgard 184, Dow Corning, Midland, MI) scaffolds or plastic cover slips in 10% fetal bovine serum (GIBCO Invitrogen) supplemented M199 medium (GIBCO Invitrogen). 24 hours later, around 50,000 non-transfected HEK293 cells, HEK293-SkM-1 cells or HEK293-SCN5A cells were added into coculture. The concentration of fetal

bovine serum was reduced to 2% in M199 medium. All the cultures were maintained in an incubator at 37℃ with 5% CO_2 for 4 to 5 days before dynamic functional measurements.

Microscopic Dynamic Functional Measurements and Analysis

All scaffolds were washed and equilibrated at room temperature in normal Tyrode's solution. The samples were then stained for transmembrane voltage with di-8 ANEPPS (Molecular Probe, Eugene, OR) for 10 minutes. After washing with Tyrode's solution for another 10 minutes, the stained samples were transferred into an experimental chamber perfused with Tyrode's solution and controlled at 30 to 32℃ to maintain a more physiologically functional environment than room temperature. The chamber was placed on an inverted microscope (Nikon TS100). Propagation measurements were performed as previously described[49]. Briefly, a Pt line electrode was placed at one end of the scaffold to pace the cells with planar waves at frequencies from 1 Hz to 2 Hz with a 0.5 Hz interval and thereafter in 0.2 Hz increments following a dynamic restitution protocol[50], until conduction was blocked. Transients of fluorescence signals were recorded at the other end of the scaffolds (around 1.1-1.5 cm from the stimulating electrode) with a photomultiplier tube (PMT). To stabilize the tissue at a steady state, for each frequency, we paced for one minute before recording. Fifteen to twenty transients were collected with IONOPTIX software at each frequency. CV was calculated as in Fig 21 and 5 transients were taken to average for each frequency.

Normal K^+ Tyrode's solution contained (in mM): NaCl 137.7, KCl 5.4, NaOH 2.3, $CaCl_2$ 1.8, $MgCl_2$ 1, Glucose 10, and HEPES 10 (pH adjusted to 7.4 with NaOH at 30℃).

High K^+ (10.4 mM) Tyrode's solution contained (in mM): NaCl 132.7, KCl 10.4, NaOH 2.3, $CaCl_2$ 1.8, $MgCl_2$ 1, Glucose 10, and HEPES 10 (pH adjusted to 7.4 with NaOH at 30℃).

Macroscopic Optical Mapping and Analysis

The macroscopic system[51] includes a CMOS camera, an intensifier, lens, excitation light and an adjustable imaging stage (Fig 31). The CMOS camera system (Cooke, Romulus, MI) has 1,280 × 1,024 pixel resolution, allowing acquisition of fast signals with high spatial resolution. An intensifier (Video Scope International, Dulles, VA) was connected to the camera, amplifying the fluorescent signal collected through a wide field of view (around 2cm) Rodenstock lens.

Samples on coverslips were washed and equilibrated in normal Tyrode's solution at room temperature. A calcium sensitive dye, fluo-4 AM (Invitrogen, Carlsbad, CA), was used to stain the cells for the measurement of AP propagation. After 20 minutes of staining, samples were washed with Tyrode's solution for another 20 minutes before the optical mapping experiments. The cover slips were then maintained in four different K^+ concentration solutions for measurement. All samples were excited at 488 nm through fiber optic light guides to record the fluorescence signal.

Propagation movies were acquired in a computer using CamWare software. Raw data of the movie were binned (2×3) and analyzed in custom-developed Matlab software. Color phase movies were generated after filtering spatially

9Gaussian, 3-pixel kernel) and temporally (Savitsky-Golay, order2, width 7). Frames at specific time points were caught by Matlab software to measure the angular velocity of the re-entrant propagation.

Normal K^+ Tyrode's solution contained (in mM): NaCl 137.7, KCl 5.4, NaOH 2.3, $CaCl_2$ 1.8, $MgCl_2$ 1, Glucose 10, and HEPES 10 (pH adjusted to 7.4 with NaOH).

10.4 mM K^+ Tyrode's solution contained (in mM): NaCl 132.7, KCl 10.4, NaOH 2.3, $CaCl_2$ 1.8, $MgCl_2$ 1, Glucose 10, and HEPES 10 (pH adjusted to 7.4 with NaOH).

7.5 mM and 9 mM K^+ Tyrode's solutions were simply made by mixing the normal and 10.4 mM K^+ Tyrode's solutions with different ratios.

RESULTS

1. Characterization of the Biophysical Properties of Na^+ Channels in SkM-1 or SCN5A Expressing Cell Lines

1.1 Generation of Na^+ channel expressing cell lines

We inserted the rat SkM-1 gene[52] or the human SCN5A gene into the pIRES2-EGFP vector (from BD Bioscience Clontech) to construct a plasmid coexpressing the α subunit of the Na^+ channel and a green fluorescent reporter gene. pIRES2-EGFP (Fig 8) contains the internal ribosome entry site (IRES) between the multiple cloning site, into which the Na^+ channel gene was inserted. It also contains the EGFP gene downstream from the same promoter. Thus, the two genes are translated into a single bicistronic mRNA so that we could identify the transfected cells by GFP examination.

We transfected human embryonic kidney (HEK) 293 cells with pIRES2-EGFP-SkM-1 or -SCN5A construct using Lipofectamine (from Invitrogen) and selected the stably transfected HEK cells by antibiotics and further sorted the GFP-positive cells by cell flow cytometry. Fig 9 shows the expression of GFP in the HEK293-SkM-1 cell line.

1.2 Comparison of the biophysical properties between SkM-1 and SCN5A in HEK293 cells

Voltage-gated Na^+ channels are responsible for the upstroke and propagation of action potentials in the conduction system of excitable tissues. Although they share similar structures and functions, cardiac and muscle Na^+

channels have different biophysical properties[45,53]. The most important difference to our study is their steady state inactivation properties. The cardiac channel has a midpoint of -74 to -80 mV[54,55], compared with a midpoint of around -68mV of the skeletal muscle channel[56]. To confirm the more positive position of the skeletal muscle Na^+ channel, we investigated the biophysical properties of these two channels in our stably transfected cell lines using whole-cell patch clamp. To better control the Na^+ current for a more accurate measurement, we used a low Na^+ (15 mM) Tyrode's solution to perfuse the cells for all Na^+ current recordings. There was a liquid junction potential of 2 to 3 mV between the bath solutions and the electrode solution. The capacitances of HEK293-SkM-1 and HEK293-SCN5A cells were 19.72 ± 0.64 pF and 21.45 ± 0.90 pF.

Activation

Fig 10 shows the voltage-dependent activation of SkM-1 and SCN5A current in the GFP positive cells. Cells were held at -100 mV to prevent inactivation, and then pulsed to test potentials from -80 mV to +40 mV, with 5 mV increments. The difference of voltages of maximal currents is about 20 mV between SkM-1 and SCN5A. According to the Nernst Equation, we calculated the equilibrium potential of Na^+

$$E_{Na} = 2.303\ (RT/zF)*\log([Na^+]_o/[Na^+]_{in})$$

and got E_{Na} = 23.31 mV at 22℃. The reversal potentials of the I/V curves of SkM-1 and SCN5A are 28.59 ± 3.04 and 18.50 ± 1.12 respectively. The peak current density and peak conductance density of are 84.53±12.39 pA/pF

and 2.19±0.32 nS/pF for SkM-1, respectively and 99.64±11.75 pA/pF and 2.05 ±0.32 nS/pF for SCN5A, respectively. T-test analysis indicated there was no significant difference in peak current density or peak conductance density between SkM-1 and SCN5A, suggesting comparable expression level of the two genes in HEK293 cells.

To study the m gate of the Hodgkin & Huxley model of these two channels in detail, we calculated the conductance at each test potential as g_{Na} = $I_{Na}/(E_{test}-E_{rev})$, where E_{rev} is the reversal potential of the I/V curve. Since $g_{Na} = m^3 h \bar{g}_{Na}$ [19], where $\bar{g}_{Na}$ is a constant and *h* is assumed as 1 because the cell was held at -100 mV, m^3 is then proportional to the conductance. Fig 11 shows the activation of the m gate: the SkM-1 channel starts to open at around -40 mV and the conductance is half maximal at -20 mV and maximal at +5 mV; the SCN5A channel starts to open at -50 mV, half maximal at -40 mV and maximal at -20 mV.

Inactivation

Next we characterized the steady-state inactivation of SkM-1 and SCN5A in HEK293 cells. Cells were prepulsed for 500 msec to a holding potential, from -100 mV to 0 mV, with a 5 mV increment, and then stepped to 0 mV. Normalized currents were fitted with the Boltzmann equation to obtain a midpoint of -53.1±0.1mV, a slope factor of 6.4 ± 0.1 mV for SkM-1 and -71.6 ± 0.5 mV, and a slope factor of 6.6±0.4mV for SCN5A (Fig 12). This relatively positive position of inactivation kinetics of SkM-1 supports the possibility that it

may function better than the cardiac Na channel to sustain conduction if cells are depolarized.

We also studied the rates of fast inactivation of SkM-1 and SCN5A. We took the slowly falling phase (starting from around 2/3 of the maximal current to full inactivation, Fig 13A) of Na^+ current measured in the activation experiment, and then fitted the data with an exponential function to get a time constant (τ) of inactivation for each membrane potential (Fig 13B). According to the Hodgkin & Huxley model of the *h* gate of Na^+ channel[19]

$$dh/dt=\alpha_h(1-h)-\beta_h h,$$

we then calculated the α and β values of the *h* gates of the two channels for each membrane potential (Fig 13C) from the expressions

$$\alpha_h = h_\infty/\tau_h,$$

$$\beta_h = (1-h_\infty)/\tau_h,$$

where h_∞ values were from the inactivation curve (Fig 12B).

Recovery

To measure the recovery of SkM-1 and SCN5A from inactivation, cells were held at a given potential and then two pulses to 0 mV were applied, with increasing time intervals between them. Data were fitted to 1 - exp ($-t/\tau$), giving a recovery time constant for each holding potential (Fig 14, 15). These time constants of SkM-1 are smaller than these for the cardiac sodium channel SCN5A at all holding potentials (Table 3), especially at more depolarized

potentials, suggesting a much faster recovery of SkM-1 which could potentially prevent slow conduction of extra stimuli leading to arrhythmia.

2. Effect of SkM-1 on the Maximal Action Potential (AP) Rate of Rise (dV/dt_{max}) of the Myocyte Coupled with SkM-1 Expressing Cells

2.1 Expression of gap junctions in HEK293 cells

To confirm the delivery ability of our delivery cell lines, that is, to confirm whether these cells can electrically couple with myocytes, we first needed to identify the expression of connexin proteins in HEK293 cells.

HEK293 cells were derived from transformation of human embryonic kidney cell cultures[57]. A previous study showed that HEK293 cells endogenously express Cx45, while Cx43 expression was undetectable[58,59]. However, our Western Blot data showed that both non-transfected and transfected HEK 293 cells expressed Cx43 and Cx45 (Fig 16). These two connexins are natively expressed in mammalian heart and can make homo- or hetero- gap junction channels[60], so expression of Cx43 and Cx45 in HEK 293 cells make it possible to couple HEK cells with myocytes.

2.2 Expression of SkM-1 improves the dV/dt_{max} in a cell-to-cell delivery model

To set up a simple cell-to-cell delivery model, myocytes disassociated from canine ventricle and HEK293-SkM-1 or HEK293-SCN5A cells were cocultured on laminin coated cover slips in M199 medium supplied with

supplements at 37℃ in a humidified atmosphere with 5% CO_2. Myocyte only culture and myocytes with non-transfected HEK293 cells were used as controls. To examine the electrical coupling between myocytes and HEK cells, we double patched myocyte-HEK cell pairs in both normal K (5.4mM) and high K (10.4 mM) Tyrode's solution at room temperature within 48 to 72 hours after plating. The gap junctional currents were identified by a symmetrical bipolar pulse protocol (400msec, from 0 to ±100mV with 20mV intervals) (Fig 17). Briefly, the protocol included two steps: first, cell pairs were stepped to various potentials from -100 to +100 mV to show the symmetry of the junctional current; second, immediately following the first step, cell pairs were stepped to the opposite polarity of the same voltages to show the recovery of the current from deactivation by reversing the gating direction. The conductance could be calculated for each junctional potential. We chose cell pairs with at least 5nS gap junctional conductance, which hyperpolarized the HEK cells toward the resting potentials of the myocytes.

With current clamping the myocytes, we measured the resting potentials and then generated action potentials by a small depolarizing stimulus (a 20 msec pulse of 20 to 40 mV). Then we compared the dV/dt_{max} of the AP measured in myocytes only, myocytes coupled with non-transfected HEK293 cells and myocytes coupled with transfected HEK293 cells expressing either SkM-1 or SCN5A (Fig 18). We plot the dV/dt_{max} of the myocytes of the four different groups versus their resting potentials. Compared with the control groups and the Myocyte-HEK293-SCN5A group with similar myocyte resting potentials, the expression of SkM-1 was associated with an increased dV/dt_{max} of the AP of

myocytes coupled with HEK293-SkM-1 cells under both normal K (5.4mM) (Fig 18B) and high K (10.4mM) (Fig 18C) conditions, suggesting that the SkM-1 currents from the HEK cells pass through gap junctions and increase the excitability of the myocytes.

To further study the effect of SkM-1 on dV/dt_{max} at different membrane potentials, we recorded the changes of dV/dt_{max} with the decrease of the membrane potentials by perfusing the cell pairs which were initially in normal K^+ solution with high K^+ solution (Fig 19). We compared the AP upstrokes of single myocytes and coupled myocytes at around -65 mV, -60 mV and -55 mV and found that SkM-1 increased the dV/dt_{max} most significantly at -60 mV (Fig 20). However, expression of SCN5A did not increase the AP upstrokes at these membrane potentials. The absence of an effect of SCN5A might result from its more negative inactivation curve which may only allow SCN5A to increase dV/dt_{max} at more hyperpolarized potentials.

Thus, our two cell delivery model suggests that SkM-1 can improve the AP upstroke and it may function better at a relatively depolarized potential around -60 mV.

3. Effect of SkM-1 on the Conduction Velocity of Action Potential Propagation in a Cell Culture Model

3.1 Generation of an *in vitro* cardiac syncytium

To set up an *in vitro* experimental preparation to study the electrical activities of cardiac tissue, we used neonatal rat cardiac myocytes. These cells

have high plasticity and can reconnect into a tissue-like syncytium after dissociation from tissue. We plated and cultured neonatal myocytes onto fibronectin-coated polydimenthylsiloxane (PDMS) scaffolds at a high density (4×10^5 cells/cm^2) to get confluent monolayers of cells. To test the effect of introducing two different Na^+ channels into the cardiac syncytium, we added around 50,000 HEK293-SkM-1 or -SCN5A cells or non-transfected HEK293 cells into the culture 1 day after plating the myocytes (with a lower density of around 3.5×10^5 cells/cm^2) and let the coculture grow for 4 to 5 days to form gap junctions and become confluent.

3.2 Expression of SkM-1 improves the conduction velocity in an *in vitro* cardiac syncytium

Since our SkM-1 expressing cells could increase dV/dt_{max} in coupled preparations, we next tested whether they could increase the speed of conduction in this *in vitro* cardiac syncytium. The syncytium we chose came from rat neonatal ventricular myocytes which may have a relatively depolarized resting potential[61].

To study propagation in our experimental preparations, we stained the cultures with a fluorescent voltage-sensitive dye, di-8 ANEPPS, and then perfused the scaffolds with Tyrode's solutions at 30℃. We paced the cultures at several frequencies from one edge of the scaffold with a platinum (Pt) line electrode. Dynamic fluorescence signals of propagated action potentials at the other edge of the scaffolds (around 1.1-1.5 cm from the electrodes) were

recorded by *Microscopic* measurements. Conduction velocity (CV) was calculated as the lag time between the stimulation pulse and acquired action potential divided by the distance (d) between the electrode and the recording site (Fig 21).

In both normal K^+ (5.4 mM) and high K^+ (10.4 mM) Tyrode's solution, CV was significantly higher in myocytes cocultured with HEK293-SkM-1 cells compared with myocytes only and myocytes cocultured with non-transfected HEK293 cells at all frequencies (Fig 22). We also compared the effects of SkM-1 and SCN5A on CV at frequencies of 1Hz, 1.5 Hz and 2 Hz (Fig 23). Although the conduction velocity of HEK293-SCN5A cell coculture was a little faster than the control myocytes, the increases were not statistically significant in either normal or high K^+ solutions. This non-effect of SCN5A may result from a relatively depolarized membranve potential of the neonatal mocytes.

Thus, our *in vitro* cardiac syncytium model suggests that introdution of SkM-1 can improve the conduction velocity better than introducing SCN5A, especially under depolarized conditions.

4. Expressing SkM-1 can Improve Conduction in an *in vitro* Arrhythmia (Reentry) Model

So far, our data demonstrated HEK293 cells expressing SkM-1 make gap junctions with cardiac myocytes, increase the maximal rate of rise of the AP and enhance its conduction velocity. Next we tested if introducing the SkM-1

channel into a cardiac syncytium under an arrhythmic condition could also increase conduction velocity and even prevent occurrence of reentry.

4.1 Setting up an in vitro arrhythmia model

We placed the same cocultures as in section **3.1** onto square fibronectin-coated coverslips and punched a hole with 0.3 cm diameter in the center of the coverslip to generate a damaged zone in the syncytium. After 4 to 5 days of culture, samples were stained with a calcium sensitive dye fluo-4 and washed with Tyrode's solution. Macroscopic optical mapping was carried out at room temperature as previously described[51] to record the fluorescence signal during AP propagation.

To introduce spiral propagation around the damaged center, we paced the culture with a point stimulator and increased the pacing frequency from 1 Hz to a certain higher frequency (around 3 to 4 Hz). With a high frequency stimulus, if the recovery of the cells was not synchronized, reentry could occur. Tyrode's solutions of four different K^+ concentrations (5.4mM, 7.5mM, 9mM and 10.4 mM) were applied in this spiral experiment. If the spiral wave could not be generated in normal K^+ (5.4 mM) condition, a higher K^+ solution was used until the conduction was low enough to induce reentrant propagation.

4.2 Expression of SkM-1 increases the angular velocity of induced re-entry

We compared the genesis of re-entry among myocyte only, myocyte-HEK293-SCN5A and myocyte-HEK293-SkM-1 cocultures and found that 4 of 7,

3 of 7 and 5 of 7 samples for each of the three groups, respectively, could not generate spirals in normal K^+ solution. Instead, spirals were induced in the 7.5 mM K^+ solution for these samples.

Although we did not see a significant difference in the ability to generate spirals in the presence of SkM-1, the propagation of the induced spirals were faster in SkM-1 culture compared with control and SCN5A culture. Raw data from macroscopic optical mapping were analyzed in custom-developed Matlab software to generate color phase movies (Fig 24). We then calculated the angular velocities (AV) of each spiral by measuring the time of 3 rotations (360° for each full rotation) and AV was presented as rotations per second. We found that AV was significantly enhanced in SkM-1 culture (Fig 25). This higher AV in SkM-1 culture may potentially terminate the propagation of the spirals because when the conduction is too fast there would be no time for the tissue to recover from inactivation.

5. Generation of a Delivery Cell Line Using Mesenchymal Stem Cells for *in vivo* Study

5.1 Creation of canine mesenchymal stem cell lines expressing Na^+ channels

Human mesenchymal stem cells (hMSCs) have been identified to express cardiac connexins Cx40, Cx43 and Cx45[40]. These cells can electrically couple with myocytes and hMSCs expressing the HCN2 gene created a biological cardiac pacemaker after injection into the canine left ventricular[44].

Considering the gene-delivery ability of mesenchymal stem cells, in this study, we chose canine mesenchymal stem cells (cMSCs) with higher viability and transfection efficiency than hMSCs as an *in vitro* delivery platform.

We tranfected cMSCs with pIRES2-EGFP-SkM-1 or -SCN5A construct using the nucleofection technique (from AMAXA). The expression of EGFP showed at least 50% transfection efficiency after 24 to 48 hours (Fig 26) and the expression lasted at lest two weeks after transfection.

5.2 Characterization of the biophysical properties of SkM-1 and SCN5A in transfected cMSCs

The Na^+ currents were measured in the GFP-positive cells perfused with a low Na^+ (15 mM) Tyrode's solution. The capacitances of cMSC-SkM-1 and cMSC-SCN5A cells were 57.63 ± 6.74 pF and 56.38 ± 6.93 pF, respectively.

Activation

Fig 27 shows the voltage-dependent activation of SkM-1 and SCN5A current in the GFP positive cMSCs. Cells were held at -100 mV to prevent inactivation, and then pulsed to test potentials from -80 mV to +40 mV, with 5 mV increments. The SkM-1 current started to activate at -40 mV, reached the half maximal value at -30 mV and peaked at -20 mV. While the SCN5A current activated at -50 mV and the half and fully maximal currents were at -40 mV and -25 mV respectively. This result suggests there was a 5 to 10 mV shift between the activation of SkM-1 and SCN5A channels. The reversal potentials of the two

currents were at 21.69 ± 1.87 mV and 21.09 ± 3.66 mV, which were close to the Nernst potential for Na^+ (+23.31 mV at 22℃). The peak current density and peak conductance density of are 38.52±4.74 pA/pF and 0.95±0.14 nS/pF for SkM-1, respectively and 55.09 ± 10.60 pA/pF and 1.27 ± 0.27 nS/pF for SCN5A, respectively. T-test analysis indicated there was no significant difference in peak current density or peak conductance density between SkM-1 and SCN5A, suggesting comparable expression level of the two genes in cMSCs.

Inactivation

Next we characterized the steady-state inactivation of SkM-1 and SCN5A in cMSCs. Cells were prepulsed for 500 msec to a holding potential, from -100 mV to 0 mV, with a 5 mV increment, and then stepped to 0 mV. Normalized currents were fitted with the Boltzmann equation. The inactivation of SkM-1 channel had a midpoint of -58.6 ± 0.4 mV, and a slope factor of 6.0 ± 0.2 mV while the SCN5A had a midpoint of -73.9 ± 0.1 mV and a slope factor of 5.9 ± 0.1 mV (Fig 28). Thus SCN5A inactivation was roughly 15 mV more negative than SkM-1. This data confirmed the relatively positive position of inactivation voltage dependence of SkM-1 suggesting CMSC-SkM-1 may also function better to deliver Na^+ current than CMSC-SCN5A if cells are depolarized.

Recovery

We also measured the recovery of SkM-1 and SCN5A from inactivation in cMSCs. Cells were held at a given potential and then two pulses to 0 mV were

applied, with increasing time intervals between them. Data were fitted to 1 - exp ($-t/\tau$), giving a recovery time constant for each holding potential (Fig 29, 30). Similar to our results in HEK239 cells, the time constants of SkM-1 are smaller than those for the cardiac sodium channel SCN5A at all holding potentials (Table 4), especially at more depolarized potentials, suggesting a much faster recovery of SkM-1 in cMSCs.

DISCUSSION

The results of our research demonstrate the differences in biophysical properties between the skeletal muscle Na^+ channel SkM-1, and its cardiac isoform SCN5A, when these two genes were exogenously expressed in selected cell lines. Importantly, the steady state inactivation of SkM-1 was about 15 to 18mV more positive than that of SCN5A. Another favorable feature of SkM-1 is faster recovery from inactivation than SCN5A. SkM-1 recovered about 1.7 to 4.3 fold faster at a membrane potential of -100 mV and about 6.2 to 13.5 fold faster at -70 mV. These characteristics of SkM-1 allow more Na^+ channels to be available at depolarized resting potentials. Consequently, in our two cell delivery model, expression of SkM-1, but not SCN5A enhanced the dV/dt_{max} of the AP upstroke in myocytes which were electrically coupled with HEK293 cells transfected with these two Na^+ channel genes. This increase was particularly significant at a depolarized membrane potential. The rate of AP upstroke directly determines the conduction velocity. At a syncytium level, we demonstrated that introducing SkM-1 into neonatal cardiac culture improves conduction velocities in both normal and depolarized conditions. In contrast, expression of SCN5A did not have any significant effect. To mimic an arrhythmic environment, we then generated an *in vitro* re-entry model with a void center. The spiral propagation induced in SkM-1 cultures showed faster angular velocity than control and SCN5A cultures, giving a potential to terminate re-entry.

In summary, our research proposed a new direction for antiarrhythmic treatment using gene and cell delivery strategy. The benefits of this new strategy

include: first, selection of a desirable gene functioning in a specific condition and second, targeting to diseased tissue with a safe, virus-free delivery method.

A Desirable Gene

The voltage gated Na^+ channel plays an important role in generation of the upstroke of the AP in that its availability determines the conduction velocity of cardiac tissue. The candidate gene we chose for this antiarrhythmic study was a Na^+ channel gene with more favorable characteristics. Compared with existing antiarrhythmic pharmacological therapies aiming to slow and block reentrant propagation, we selected this gene to speed conduction, which was not just simply opposite to previous methods, but worked better in a depolarized condition often associated with an arrhythmic environment.

Choosing between the cardiac and skeletal muscle Na^+ channel genes

There are many differences between the biophysical properties of the skeletal muscle and the cardiac Na^+ channels, such as the potentials at which activation reaches maximal values, the half points of inactivation (h_∞) curves[62]. The kinetics of activation and inactivation are also quite different between these two isoforms, for examples, the time to reach half of the maximal current amplitude and the time constants of recovery from inactivation[63]. Our results confirmed these differences in exogenously expressing cell lines. In HEK293 cells, SkM-1 reached a maximal current amplitude at -10 mV while SCN5A

reached its half maximal value at -35 mV. The half points of steady state inactivation curve of the two channels were -53 mV and -72 mV. In cMSCs, the potentials of maximal current were -20 and -25 mV and the half points of inactivation were -59 and -74 mV for the two isoforms, respectively. Differences exist not only between species, but it has been reported that these characteristics also depend on the cells in which they are expressed[62]. In our case, both activation and inactivation of the two channels were a little more positive in HEK293 cells compared with cMSCs. These might be related to differential expression of auxiliary subunits or the effects of temperature. Indeed, the steady state inactivation curve was found to be more hyperpolarized at lower temperature[64,65]. Possibly this may explain the relatively more positive position of the inactivation curve in all of our results recorded at room temperature compared with other studies at lower temperature or in different expression systems.

A favorable inactivation

Among all the electrophysiological features of the voltage gated Na^+ channel, inactivation is the one most important to cell excitability. It determines the pool of available Na^+ channels to fire the AP. Two types of inactivation with different kinetics have been observed in the Na^+ channels: fast inactivation within milliseconds and slow inactivation on the order of seconds[66]. These two separate processes involve different regions of the channel and different mechanisms to inactivate[67]. Although both of the processes may regulate the resting state of Na^+

channels and the duration of the AP, in our case, we simply used the Hodgkin and Huxley model (which describes the fast component of inactivation) to study the steady state inactivation because introduction of SkM-1 into cardiac tissue did not increase the AP duration[68] suggesting little if any slow inactivation.

In HEK293 cells, we obtained an 18 mV difference between the steady state inactivation curves of SkM-1 and SCN5A. At -90 mV, both of them have most of their channels available. At -60 mV, there were about 73% of SkM-1 but only 13% of SCN5A available. While at -50 mV, most of SCN5A were inactivated but around 37% of SkM-1 channels were still available. This difference was a little bit smaller in cMSC cell lines. The midpoint of SkM-1 inactivation was 15mV more positive than that of SCN5A. At -60 mV, 57% compared with 7% of the channels were available. So the fraction of available Na^+ channels at depolarized potentials was much higher in cells expressing SkM-1 than those expressing SCN5A.

In addition, comparing the fast inactivation between SkM-1 and SCN5A, we observed a slower kinetics for SCN5A. This difference may result from modulation of the C-terminal domain of the SCN5A channel[69]. The “faster” fast inactivation of SkM-1 may provide another benefit to prevent long QT syndrome.

A favorable recovery

Recovery from fast inactivation is also an important characteristic that contributes to the availability of Na^+ channels for AP propagation. Our results showed that at -100 mV, the time constants of recovery of SkM-1 and SCN5A

were 1.7 and 7.3 msec in HEK293 cells, respectively, and were 3.9 and 6.3 msec in cMSCs. The time constants of recovery at -70 mV of these two channels were 5.2 and 69.8 msec in HEK293 cells and 16.4 and 101.4 msec in cMSCs, respectively. So at a relatively depolarized potential, SCN5A may take more time to recover than SkM-1 by one order of magnitude.

This faster recovery of SkM-1 may preserve propagation particularly at high frequency stimulation. However, it may have both advantages and disadvantages in avoiding reentrant propagation. On one hand, it may prevent re-entry from happening. On the other hand, it might be difficult to stop existing re-entry because of the faster recovery from inactivation of the tissue. Nevertheless, this fast recovery from inactivation unambiguously speeds conduction in all circumstances.

Other choices

As the structure-function relationship of the Na^+ channel has been studied by mutagenesis at specific sites, more is known about the critical amino acid residues which play important roles in the biophysical properties. Change of a single residue may result in a difference in functional behavior, such as inactivation[70]. These studies may not only help us to learn more about the molecular mechanisms of Na^+ channels, but also offer the opportunity to generate desirable genes that target specific uses. According to mutagenesis studies, we can genetically modify existing channels at relevant locations to obtain more favorable biophysical properties. For example, a mutant G1306E of

the skeletal muscle Na^+ channel has been well studied in inherited human myotonia[71]. This mutant has an even more positive steady state inactivation than the wild type, which can enhance cell excitability. Therefore, by understanding more and more about the structure of Na^+ channels related to their function, we can find other candidates for antiarrhythmic gene therapy.

A Safe Cell Delivery Platform

Advantages of using cell delivery system

Because of the ability to insert their own genes into the chromosome of host cells, viruses have been commonly used as vectors to transfer genes into target cells. However, several problems prevent viral gene therapy from becoming an effective and safe treatment[72]. First, immune responses might be stimulated after viral infection. Second, retrovirus vectors may integrate into genome at any location, which yields a danger for mutagenesis and tumorigenesis[73]. Third, adenoviruses might be safer vectors but have the problem of short-lived expression. In addition, disadvantages of toxicity, inflammation and uncontrolled viral replication or mutation also limit the therapeutic use of gene therapy.

In contrast, a cell delivery system may overcome some of these problems. We can use the patient's own stem cells to introduce genes, which should reduce the risks of immunoresponse and toxicity. Furthermore, we can thoroughly study the functional properties of the gene of interest in the expression cell line before introducing it into the target tissue.

Introducing Na^+ current through gap junction

Our strategy to deliver the Na^+ channel into the cardiac tissue is through gap junctions provide the electrical connection between myocytes to conduct the AP in the heart. Three major isoforms of connexin proteins Cx43, Cx45 and Cx40 are prominently expressed in the heart. Each of these connexins shows different channel properties and regional specific expression[74]. Cx43 is the only connexin abundantly expressed in the working ventricular myocardium[75]. Cx45 forms gap junctional channels with very low conductance, and is localized in the nodes and His bundles and Purkinje system[76]. Cx40 is found in His-Purkinje system with high conductance[77]. This compartmentalized pattern of connexin expression contributes to the organized, orderly conduction in the heart.

To introduce the desirable Na^+ channel to the cardiac tissue, the delivery cells need to electrically couple with the myocytes. We hypothesized that the Na^+ current passing through the membrane of the delivery cell also enters into the myocyte through gap junction during generation of the AP, so that the AP upstroke can be enhanced. We demonstrated the expression of Cx43 and Cx45 in HEK293 cells and our double patch clamp data showed gap junction formation between the ventricular myocyte and the HEK293 cell.

Previous studies have shown that homotypic gap junction channels, in which both hemichannels are composed of the same connexins, generate symmetrical voltage dependent junctional currents; while heterotypic channels, in which each of the hemichannels is composed of a different connexin, show asymmetrical voltage dependency[78,79,80]. There are also heteromeric channels in

which each hemichannel contains at least two different connexins[81]. We observed both asymmetrical and symmetrical behaviors of the junctional currents between myocytes and HEK293 cells. Since the myocytes were derived from canine ventricle where Cx43 was highly expressed and HEK293 cells expressed both Cx43 and Cx45, the gap junctions between these two cells might be either Cx43 homotypic or Cx43/Cx45 heterotypic.

Effects of Introducing the Desirable Gene SkM-1 with the HEK293 Cell Delivery System on Cardiac Conduction

Effect on the AP upstroke

The upstroke of the AP determines the cardiac conduction velocity and its maximal rate of rise (dV/dt_{max}) is directly determined by the excitatory inward currents. So, measuring the effect of expression of SkM-1 on the dV/dt_{max} was the first step in testing its antiarrhythmic potential.

Our results showed that the dV/dt_{max} was significantly increased in the myocyte coupled with a HEK293-SkM-1 cell. To generate a depolarized condition, we used a 10.4 mM K^+ solution to decrease the cell resting potentials. We found that the dV/dt_{max} was also increased in SkM-1 cell pairs in the high K^+ solution. Analysis of the change of dV/dt_{max} with membrane potential showed that the increases by SkM-1 were most significant at around -60mV and -55mV, with a ratio of 1.5 fold and 2.5 fold respectively. These results are consistent with the inactivation curve of SkM-1 we obtained from HEK293 cells. At these voltages, there were big differences of available Na^+ channels between SkM-1 and SCN5A.

We did not see an effect of SCN5A on the dV/dt_{max} in myocytes coupled with HEK293-SCN5A. Since the current densities of SkM-1 and SCN5A were similar in the two stable cell lines, the absence of an effect of SCN5A is not due to lower expression of SCN5A. Rather, myocytes in primary tissue culture condition may have relatively lower resting potentials due to decreases of the inwardly rectifying current (I_{k1})[82], most of our cultured myocytes showed membrane potentials between -65 and -68 mV. We assume expression of SCN5A may function effectively at more hyperpolarized potentials which our culturing condition did not reach.

Effect on the conduction velocity of an in vitro cardiac syncytium

After demonstrating that SkM-1 increases the AP upstroke, we then tested the effect of SkM-1 on conduction velocity. Rat neonatal myocytes were used to generate an *in vitro* cardiac syncytium. We found that coculturing myocytes with HEK293-SkM-1 cells could enhance the conduction velocity of the syncytium under both normal (5.4mM K^+) and depolarized (10.4mM K^+) conditions. The ratio of myocytes and HEK293 cells might be critical to the effects of SkM-1 expression. At the beginning of coculture, we loaded around 50,000 HEK293 cells into 4.5×10^6 myocytes. The doubling time of HEK293 cells is around 2 days. With 5 to 6 days of coculture, the final ratio of myocytes to HEK293 cells reached around 10:1. More HEK293 cells loaded into the coculture may have resulted in a depolarization of the whole syncytium so that more Na^+

channels including the introduced SkM-1 channels are inactivated leading to decreased conduction velocity.

Again, we did not see a significant increase in the conduction velocity in the SCN5A culture under either normal or depolarized conditions. This result may also be due to the relatively positive resting potential of rat neonatal ventricular myocytes.

Effect on the conduction of an in vitro re-entry model

Because many tarchyarrhythmias are associated with a re-entrant mechanism, we then set up an *in vitro* re-entry model by high frequency stimulation to test if SkM-1 could also function in an arrhythmic situation. Although SkM-1 did not prevent re-entry, we found that the SkM-1 coculture has a faster angular velocity of the induced re-entry than the control and SCN5A cultures under both normal and depolarized conditions, which suggests the potential of SkM-1 to terminate the re-entrant propagation. Indeed, a recent *in vivo* study in a canine model of myocardial infarction supported the antiarrhythmic potential of SkM-1[68]. The adenovirus containing SkM-1 gene was injected into the epicardial border zone (EBZ) of the infarcted animal. Five days after injection, the SkM-1 treated animals showed narrower electrograms than the control (indicating a higher CV). And introducing SkM-1 prevented induced VT/VF by premature stimulation. Also, the myocytes from the SkM-1 injected EBZ showed increased dV/dt_{max} of the AP.

LIMITATIONS AND FUTURE DIRECTIONS

There are several questions we need to consider for future study:

1) Slow inactivation of SkM-1: it has been reported that the skeletal muscle Na^+ channel has a greater probability of slow inactivation than the cardiac channel[83]. Although our steady state inactivation study showed a higher availability of SkM-1 at depolarized potentials, the 500 msec prepulses of depolarization could not separate the fast and slow components of the inactivation. Because our data and two other relevant studies[68,84] showed the more favorable antiarrhythmic effect of SkM-1 at depolarized potentials and introducing SkM-1 into myocytes did not prolong the AP duration, it seems likely that there is only a small fraction of SkM-1 channels undergoing slow inactivation although we could not exclude its presence. In addition, a single residue mutation can largely reduce the probability of slow inactivation of SkM-1[70]. So, if slow inactivation does become a problem in future studies, a mutant of SkM-1 can be generated with more desirable properties.

2) Faster recovery of SkM-1: this property might be both an advantage and a disadvantage for the antiarrhythmic effect of SkM-1. Faster recovery is always good for normal high frequency impulse conduction. The research in this dissertation does not address the function of SkM-1 to preserve conduction at high frequency. In addition, in the re-entry model, if the SkM-1 culture recovers faster, we should have seen spiral propagation induced at higher frequencies than control. However, because of the variance between samples our

experimental approach limited our ability to detect this effect. On the other hand, once the spiral propagation is generated, faster recovery of SkM-1 may prevent it from stopping.

3) Gap junction expression for delivery efficiency: HEK293 cells have a resting membrane potential of -20 to -30 mV. To allow the SkM-1 channel to avoid steady state inactivation, sufficient gap junction channels need to be open so that the HEK293 cells can be hyperpolarized by the myocytes. We did not address the question of what magnitude of gap junctional conductance is required to hyperpolarize the HEK293 cells. Also, the effect of SkM-1 on dV/dt_{max} of the AP might be regulated by the conductance between the cell pairs. Because of the difficulty of the double patch clamp and the variance of resting potentials among cultured myocytes, it is difficult to determine this relationship. Furthermore, for the *in vitro* cardiac syncytium, immunostaining for Cx43 and Cx45 may help us to test the expression of gap junctions between myocytes and HEK293 cells.

4) Mesenchymal stem cells as delivery system for *in vivo* study: we have identified the more favorable biophysical properties of SkM-1 when expressed in canine mesenchymal stem cells. Before *in vivo* studies, the effect of cMSC-SkM-1 cell on conduction velocity of the *in vitro* model needs to be tested. The expression of connexin proteins between myocytes and cMSCs will be measured by immunostaining. Considering that cMSCs are larger than HEK293

cells, the membrane potential of myoctes might be depolarized by cMSCs so as to reduce the effect of SkM-1. Therefore, the ratio of myocytes to cMSCs in the coculture needs to be adjusted. In addition, an inwardly rectifying channel (I_{k1}) may be introduced into cMSCs to hyperpolarize their resting potentials.

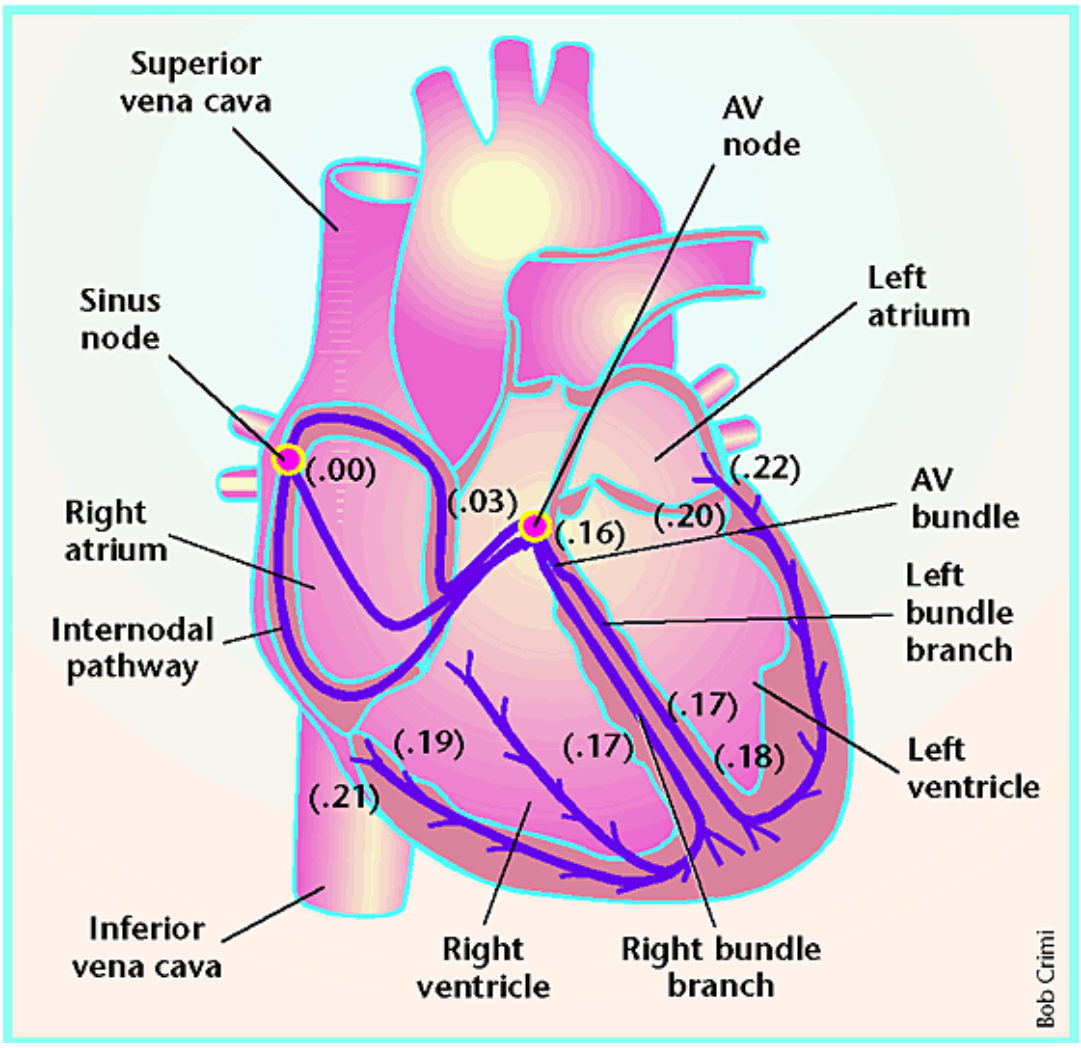
Superior vena cava
AV node
Left atrium
Sinus node
(.00)
(.03)
(.16)
(.20)
(.22)
AV bundle
Right atrium
Left bundle branch
Internodal pathway
(.17)
(.19)
(.17)
(.18)
Left ventricle
(.21)
Inferior vena cava
Right ventricle
Right bundle branch
Bob Crimi

Figure 1. (Jeffrey Robbins & Gerald W Dorn II, 2000) Cardiac conduction system[1].

Impulses are spontaneously emitted from the sinus (SA) node which is directly connected to the atrial fibers. So the action potential immediately spread through the entire atrial muscle mass. Signals are transported to the atrial-ventricular (AV) node through specialized conducted bundles within 30 msec. Slow conduction in the AV node generates a delay of ~130 msec allowing the atria to contract and fill up the ventricle. The conducting action potential is then propagated through the bundles of His and Purkinje fibers of the ventricular conduction system. These fibers have a fast conduction velocity transmitting the impulse at 3−5 m/s. So, the signal propagates through the entire His-Purkinje system within 60 msec, ensuring a synchronous contraction of the ventricles and the ejection of blood.

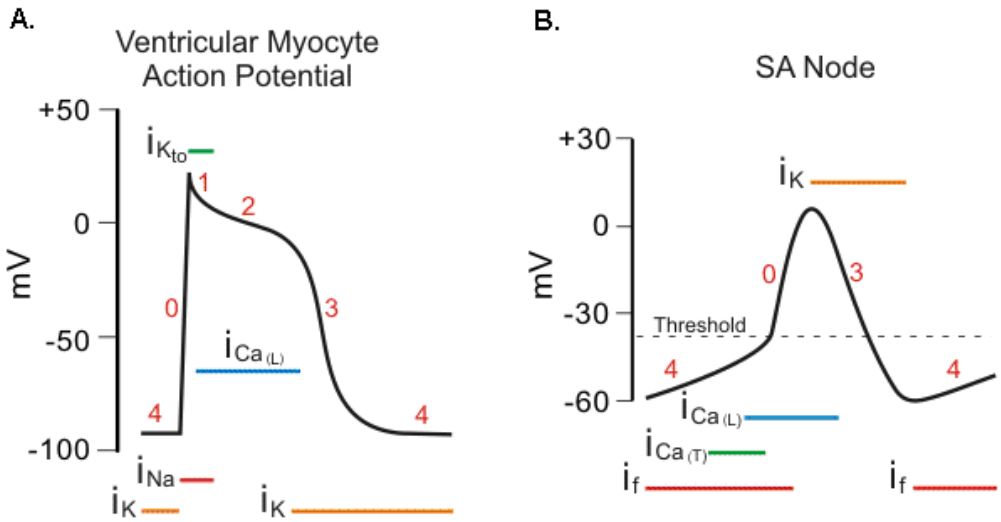

Figure 2. The action potentials of a ventricular myocyte and a SA nodal cell. (From: www.cvphysiology.com)

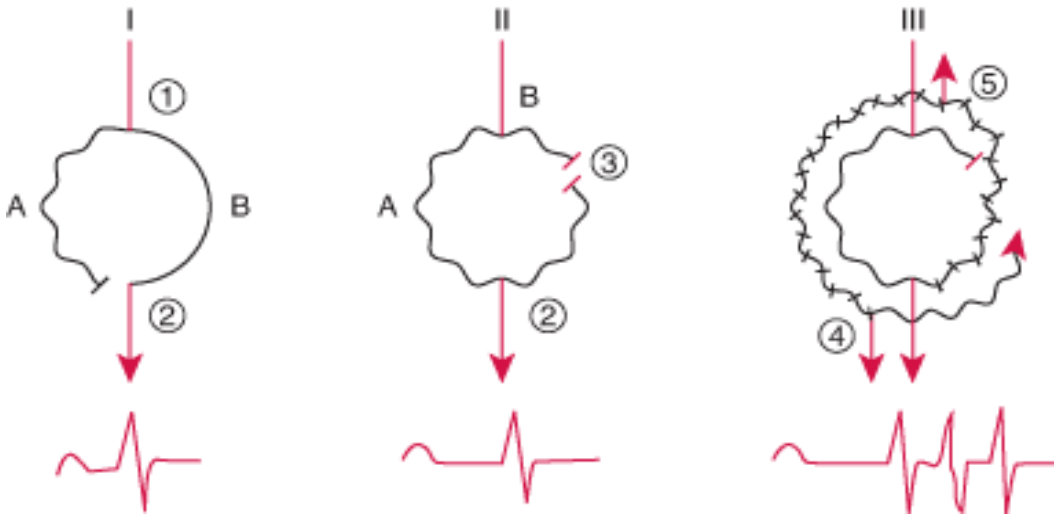

Figure 3. Mechanism of typical reentry. (From the Merck Manuals Online Medical Library: www. Merck.com)

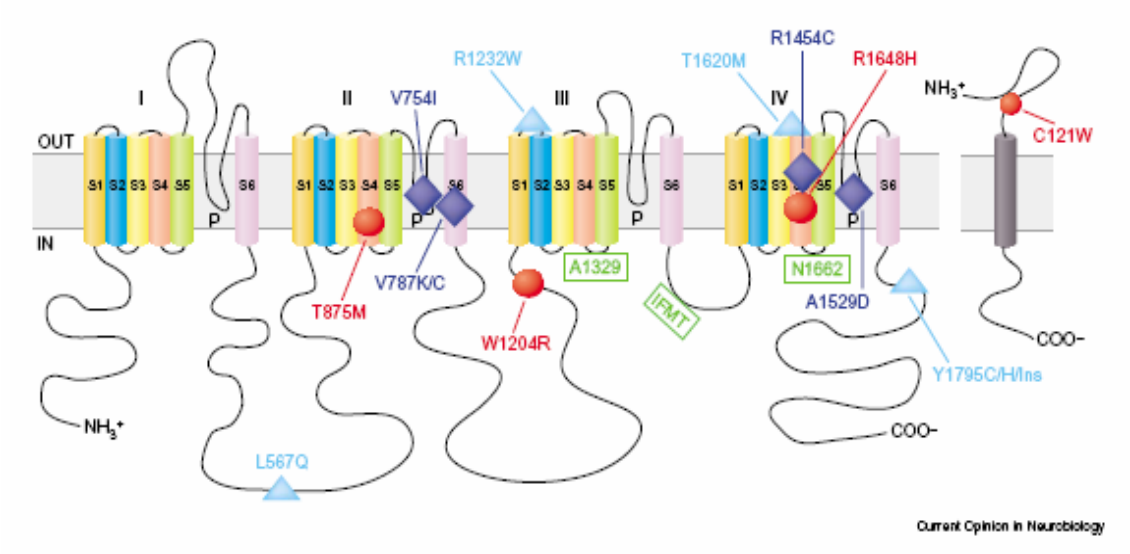

Figure 4. Structure of the α subunit of Na^+ channel[67].

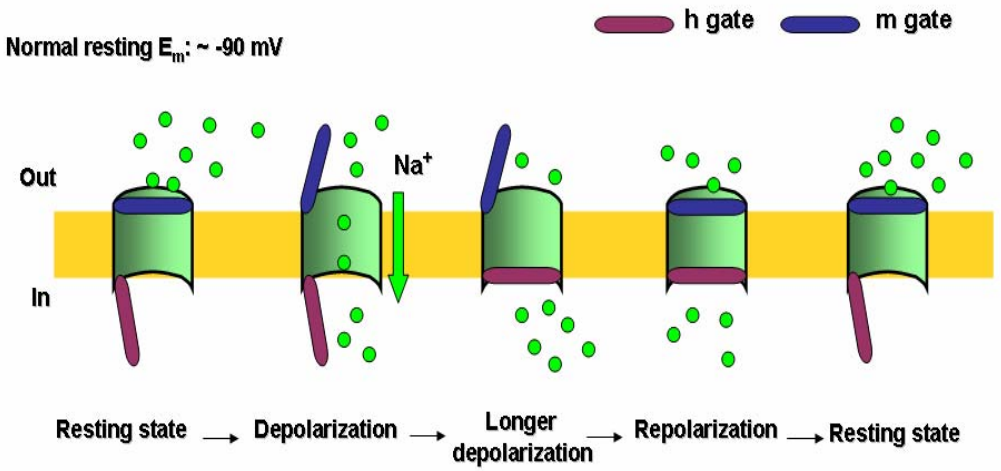

Figure 5. The Hodgkin and Huxley model for gating Na^+ channels.
At a normal resting potential, which is around -90 mV in a myocyte, the h gate of the channel is in an open state. A depolarizing stimulus results in rapid opening of the m gate allowing Na^+ into the cell to generate the action potential. Further depolarization slowly closes the h gate leading to an inactivated state. Repolarization rapidly closes the m gate and re-opens the h gate, bringing the channel back to a resting but activatable state.

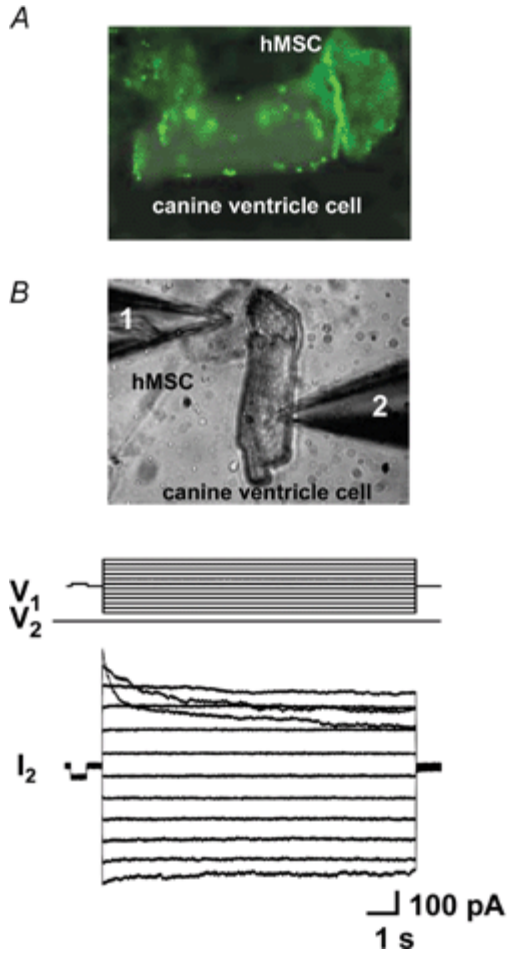

Figure 6. Expression of gap junctions between hMSC-canine ventricle cell pairs[40]. **(A)** Immunostaining of Cx43 expression between the ventricular myocyte and the human mensenchymal stem cell. **(B)** Gap junctional current between the cell pair.

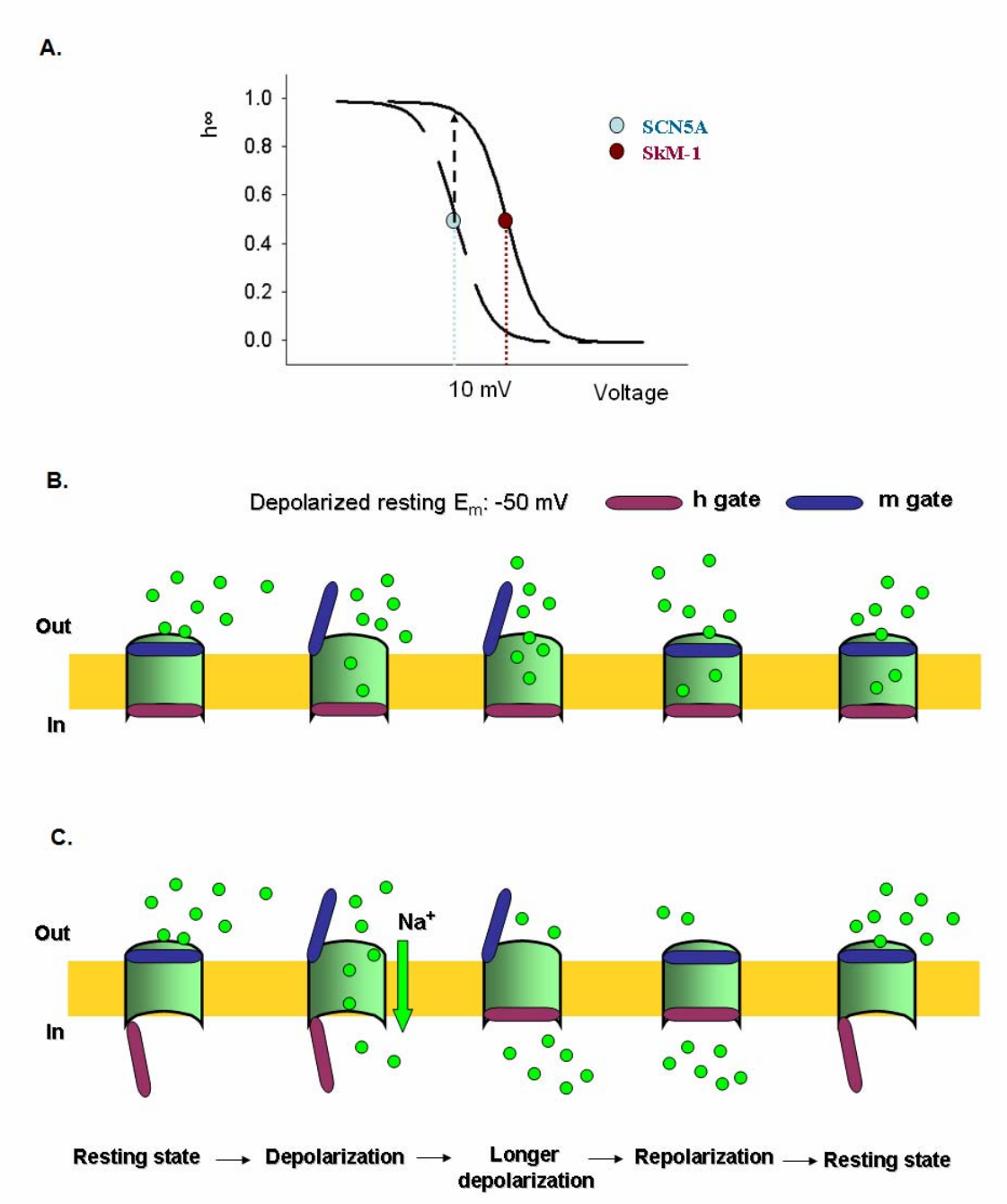
A.
h∞
1.0
0.8
0.6
0.4
0.2
0.0
SCN5A
SkM-1
10 mV
Voltage
B.
Depolarized resting Em: -50 mV
h gate
m gate
Out
In
C.
Out
In
Na+
Resting state
Depolarization
Longer depolarization
Repolarization
Resting state

Figure 7. Comparison of voltage dependent inactivation between SCN5A and SkM-1 and their availability at depolarized resting potentials. (A) A 10 mV more positive SkM-1 inactivation curve compared to that for SCN5A may allow more Na^+ channel availability at a depolarized potential (dashed line). **(B)** Most of the SCN5A channels have their h gates closed at a resting potential around -50 mV, so that the channels are inactivated leading to unavailability of Na^+ currents for generation of the action potential. **(C)** The h gates of more SkM-1 channels are in the available state because of its more positive inactivation curve. Further depolarization opens the m gate allowing Na^+ ions through.

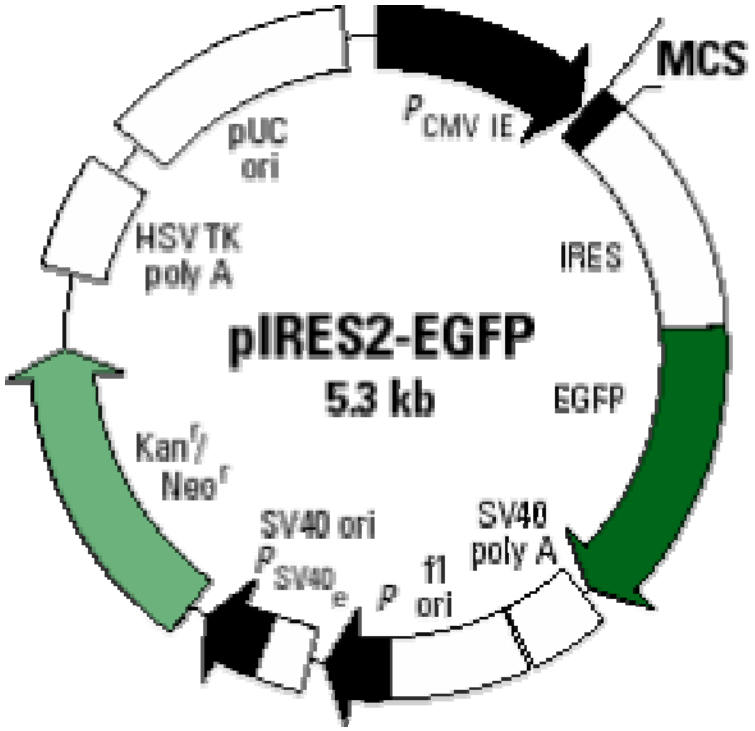

Figure 8. Map of pIRES2-EGFP vector. Rat skeletal muscle sodium channel (SkM-1) and human cardiac sodium channel (SCN5A) were inserted into the multiple cloning site (MCS) of the vector.

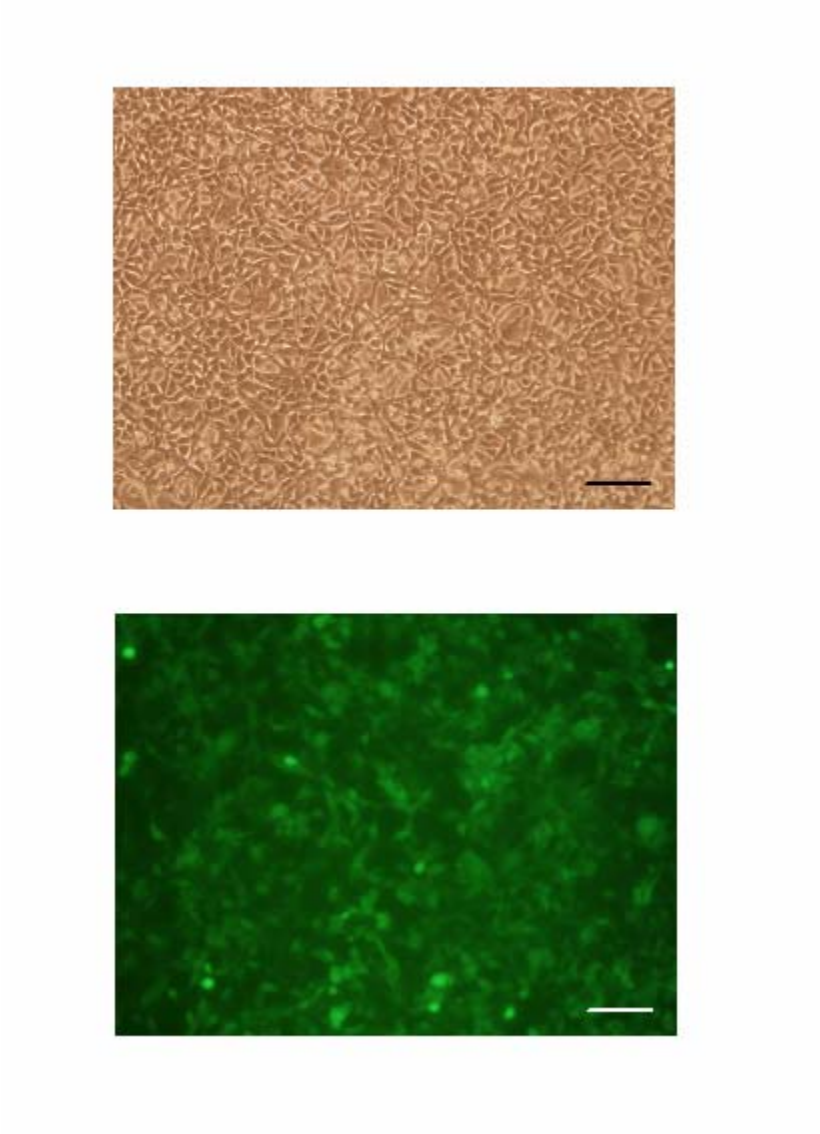

Figure 9. Cultured HEK293-SkM-1 stable cell line after GFP sorting. The upper panel shows phase contrast image of HEK293-SkM-1 cells. The lower panel shows GFP expression. Fluorescence was stably detected for at least 20 passages. (Scale bar: 200 μm)

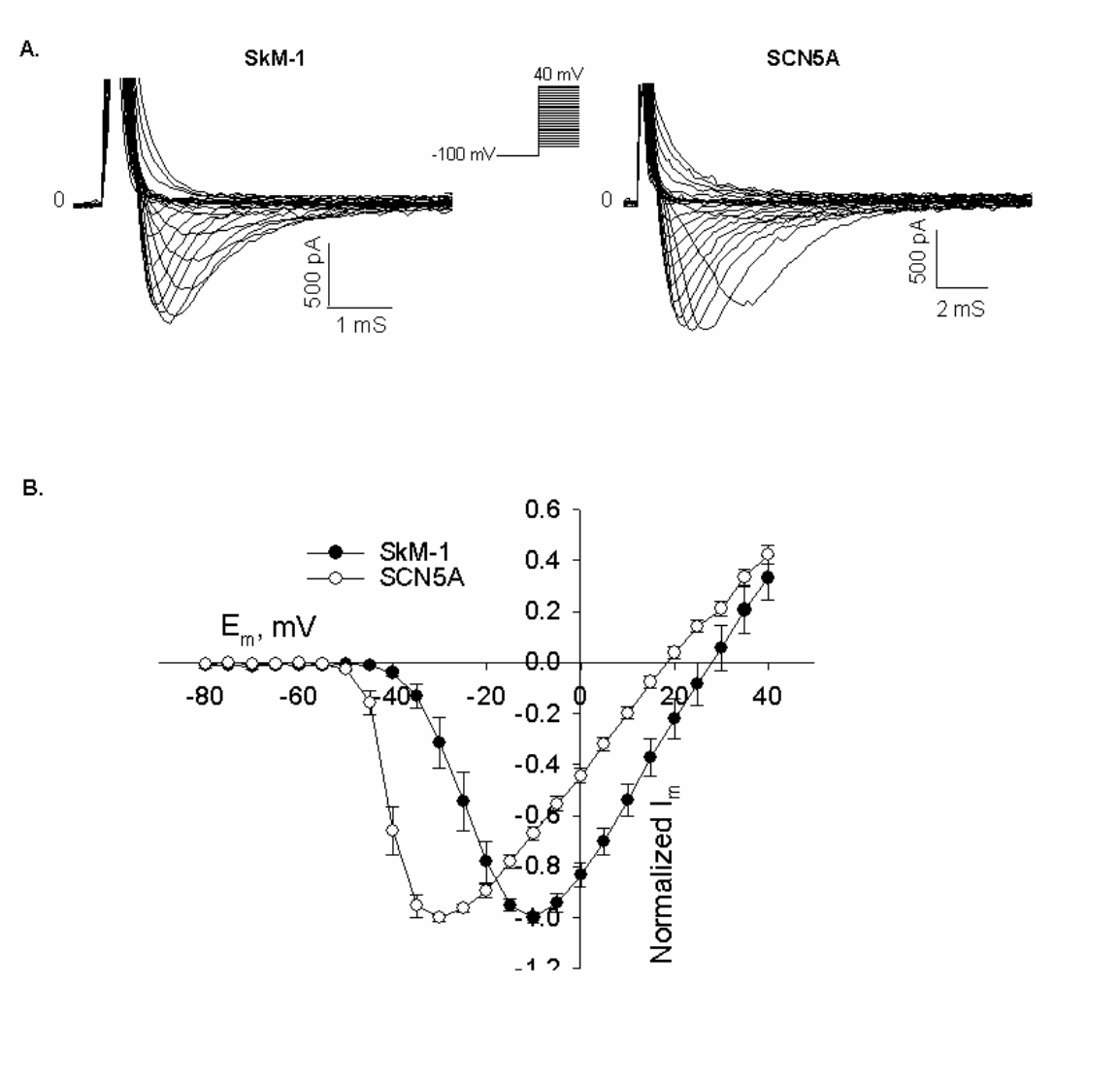

Figure 10. Activation of SkM-1 and SCN5A in HEK293 cells. (A) Expression of SkM-1 or SCN5A in HEK293 cells. Na^+ currents were recorded in low Na^+ (15 mM) Tyrode's solution at room temperature. **(B)** Current-voltage relationship of SkM-1 (n=8) and SCN5A (n=10) in HEK293 cells. Cells were held at -100 mV and then pulsed to test potentials from -80 mV to +40 mV, with a 5 mV increment. Data are normalized to the maximum peak current (mean±SE). The peak current densities of SkM-1 and SCN5A were 84.53± 12.39 and 99.64±11.75 pA/pF, respectively.

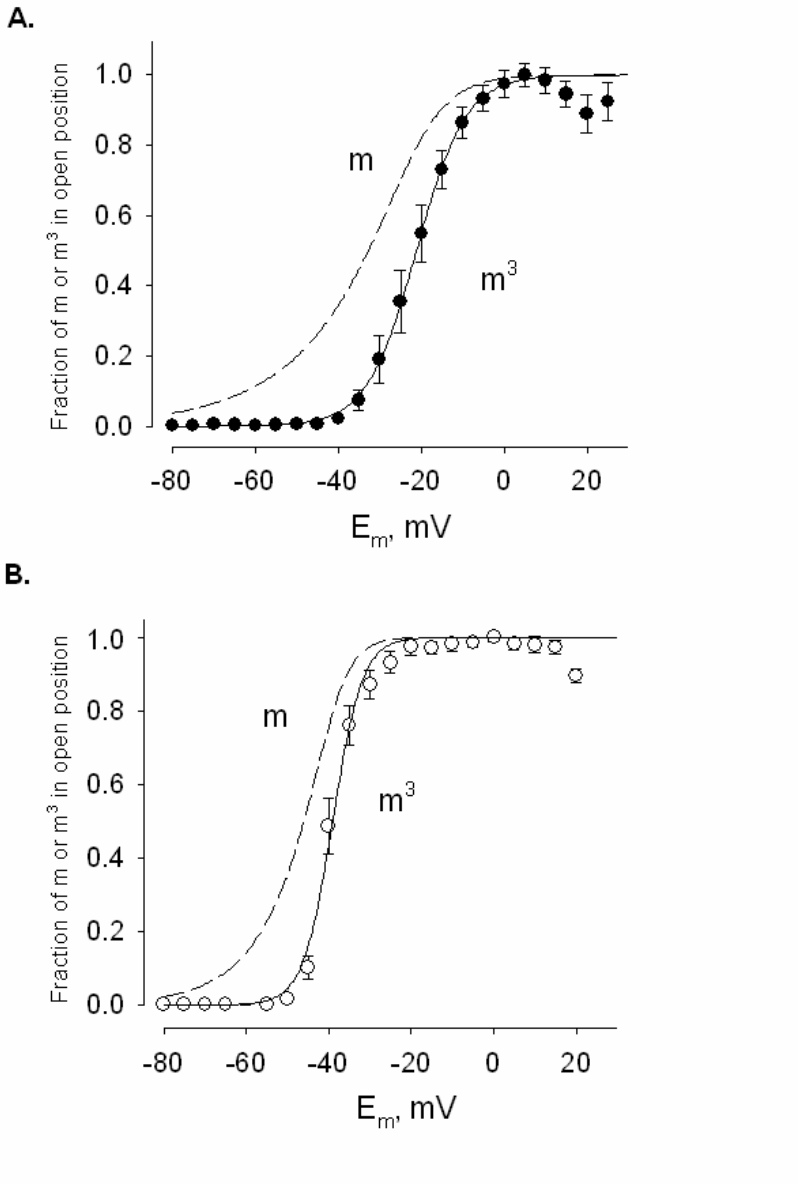

Figure 11. Study of the m gates of SkM-1 and SCN5A. Data of m^3 are normalized to the maximal value and fitted to the equation $f = \frac{1}{1+\exp[-(Em-Vh)/K]}$, giving a midpoint of -21.1±0.5 mV and a slope of 5.9±0.4 mV (mean±SE, n = 8) for SkM-1 **(A)**, and a mid point of -39.0±0.4 mV and a slope of 3.6±0.4 mV (mean±SE, n = 10) for SCN5A **(B)**. The m curves were calculated from the curve fit.

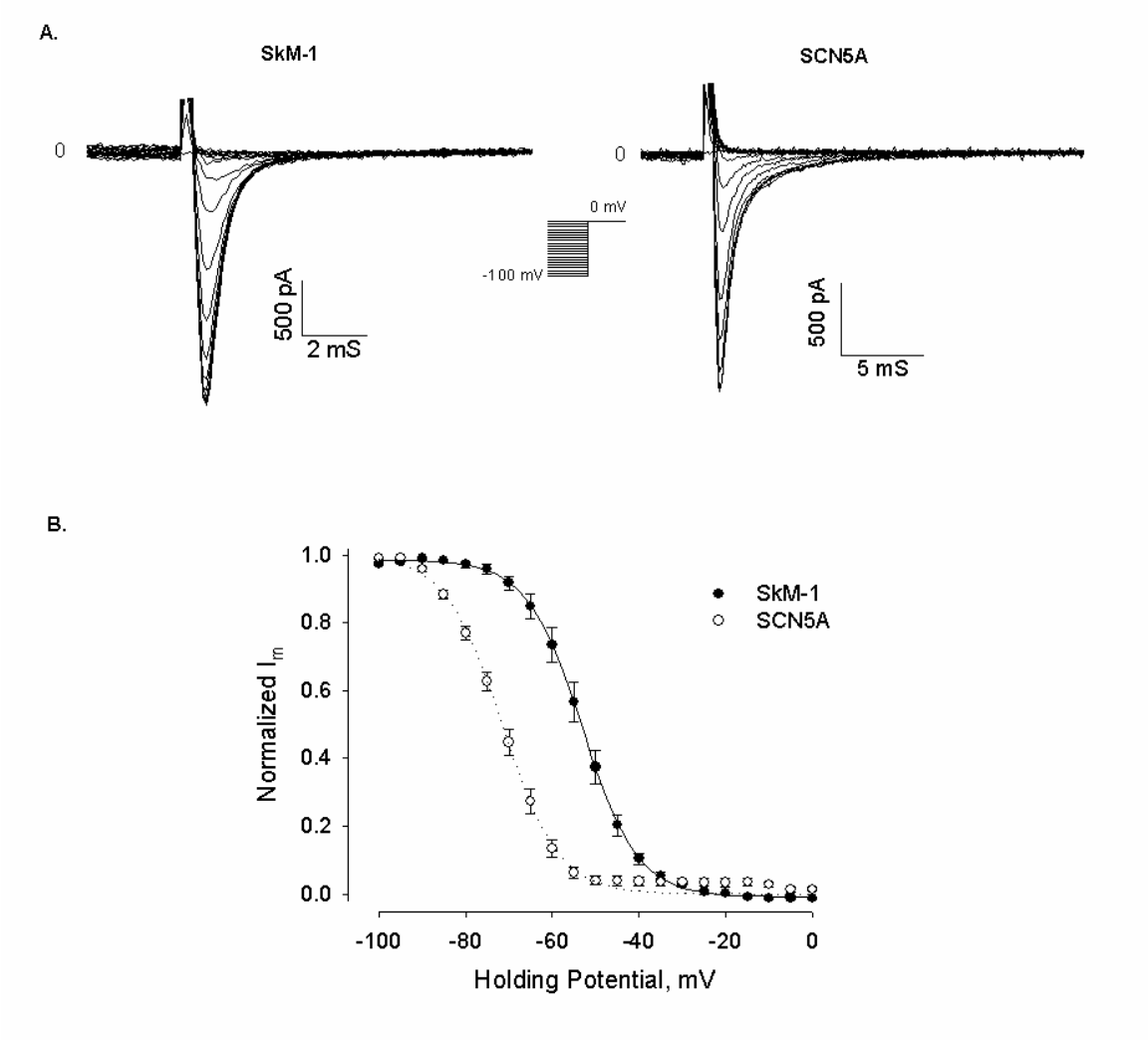

Figure 12. Inactivation of SkM-1 and SCN5A in HEK293 cells.
(A) Representative inactivation of SkM-1 and SCN5A currents in HEK293 cells. Cells were held at different holding potentials from -100 mV to 0 mV for 500 msec, with a 5 mV increment, and then pulsed to 0 mV. **(B)** The inactivation curve (the h_∞ curve) of SkM-1 (n=12) and SCN5A (n=10). Data are normalized to the maximum peak current and fitted to the Boltzmann equation $f = \frac{1}{1+\exp[(Em-Vh)/K]}$, where V_h is the midpoint membrane potential and K is the slope factor (mean±SE).

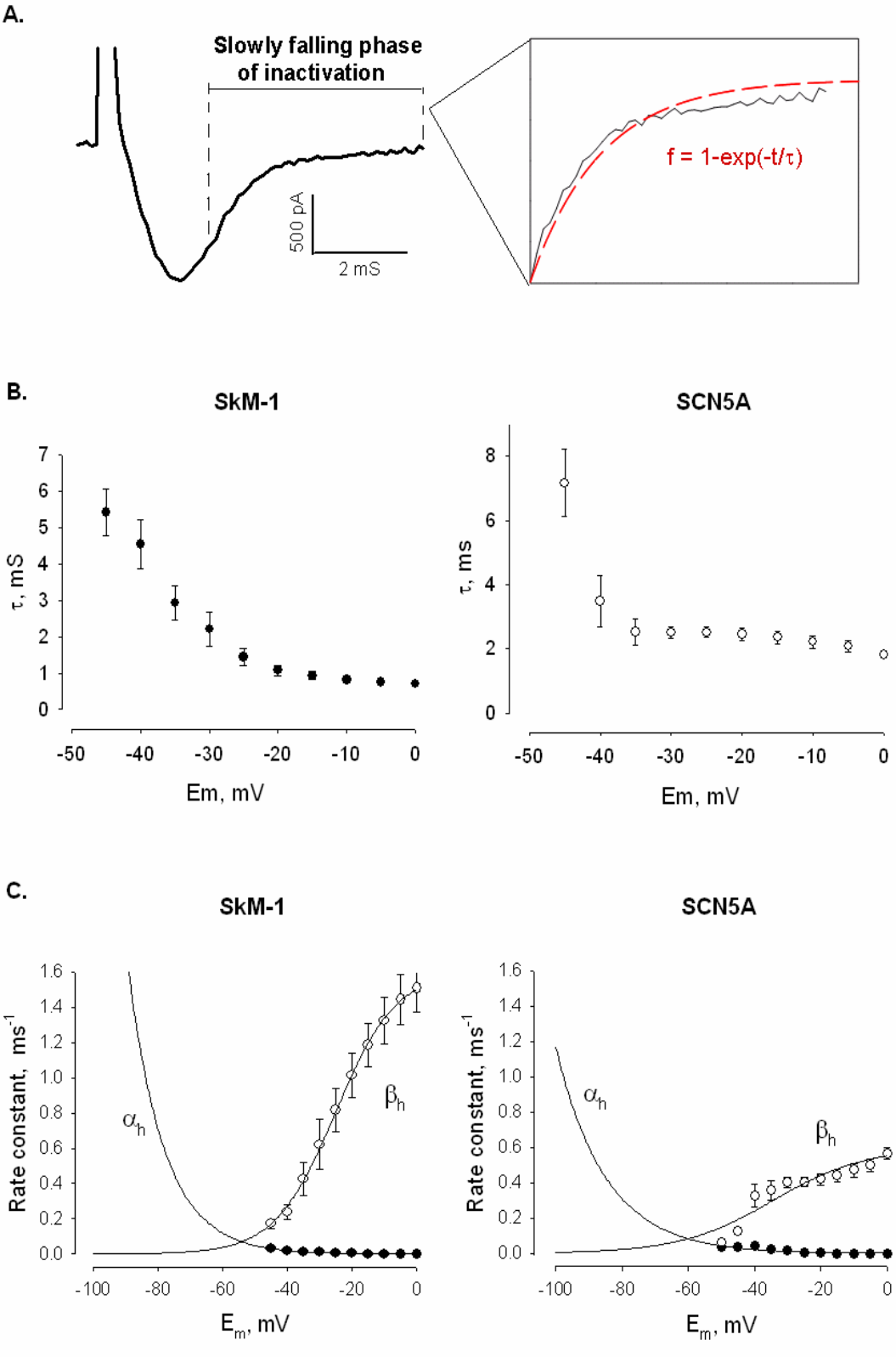
A.
Slowly falling phase of inactivation
500 pA
2 mS
f = 1-exp(-t/τ)
B.
SkM-1
SCN5A
τ, mS
τ, ms
Em, mV
Em, mV
C.
SkM-1
SCN5A
Rate constant, ms-1
Rate constant, ms-1
αh
βh
αh
βh
Em, mV
Em, mV

Figure 13. Study of the *h* gates of SkM-1 and SCN5A. (A) Inactivation of a representative Na^+ current, starting from 2/3 of the maximal current to full inactivation. **(B)** The time constant (τ) for each membrane potential of the h gate of channels was obtained by fitting the inactivation phase with an exponential equation $f = 1\text{-}\exp(-t/\tau)$. Data are presented as mean ± SE, n = 8 and 6 for SkM-1 and SCN5A, respectively. **(C)** Calculated α and β values of the h gate of the two channels for each membrane potential. α_h values were curve fit by $\alpha_h = a*\exp(-b*E_m)$, where a = 5 ± 2 × 10^{-4}, b = 0.09 ± 0.01 for SkM-1; a = 1.5 ± 1.4 × 10^{-3}, b = 0.07 ± 0.02; β_h values were curve fit by $\beta_h = a/(1+\exp(-\frac{Em-E0}{b}))$, where a = 1.60 ± 0.03, b = 9.37 ± 0.32 and E_0 = -25.16 ± 0.45 mV for SkM-1; a = 0.60 ± 0.10, b = 14.02 ± 5.62 and E_0 = -34.48 ± 6.34 mV for SCN5A.

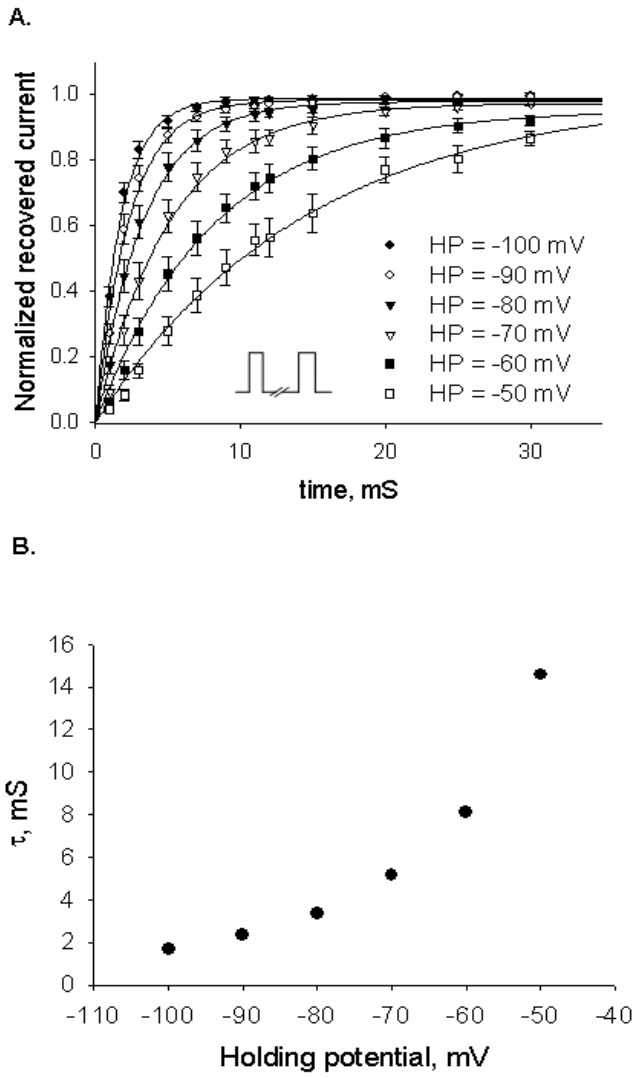

Figure 14. Recovery of SkM-1 in HEK293 cells. Cells were held at a holding potential and double-pulsed to 0 mV. Each pulse had a 10 msec duration, with an increasing time interval between the two pulses. Data were normalized to the current value of the first pulse (mean±SE, n = 8 for each holding potential) and curve fit the equation $f = 1- \exp(-t/\tau)$.

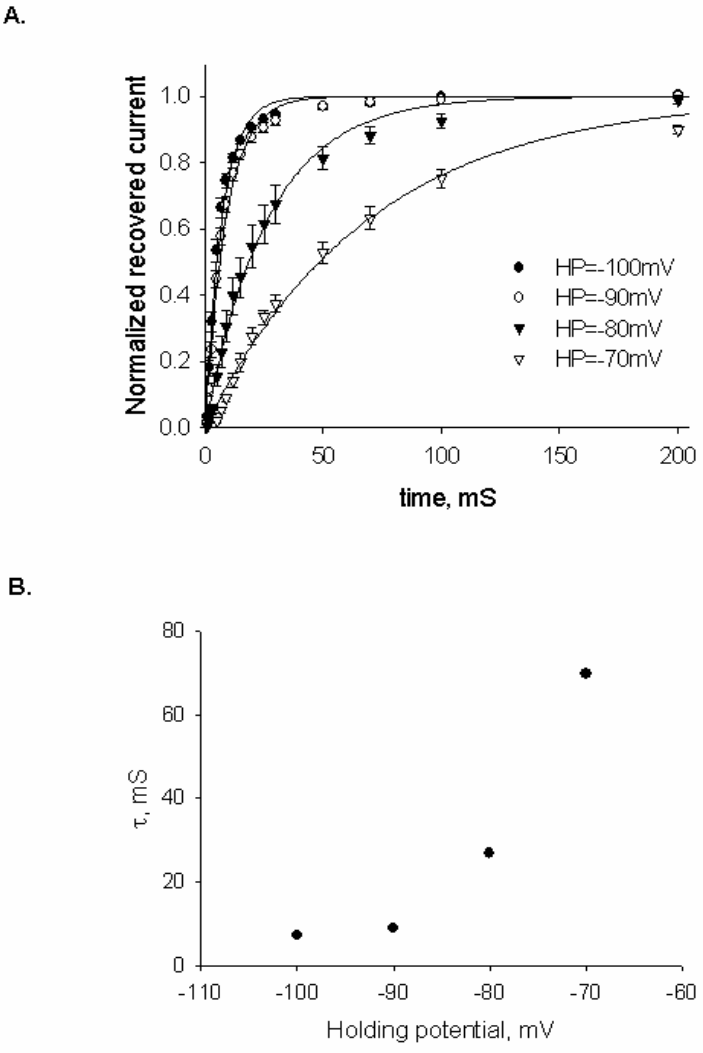

Figure 15. Recovery of SCN5A in HEK293 cells. Data were normalized to the current amplitude of the first pulse (mean ± SE, n = 8 for each holding potential) and curve fit to the equation $f = 1 - \exp(-t/\tau)$.

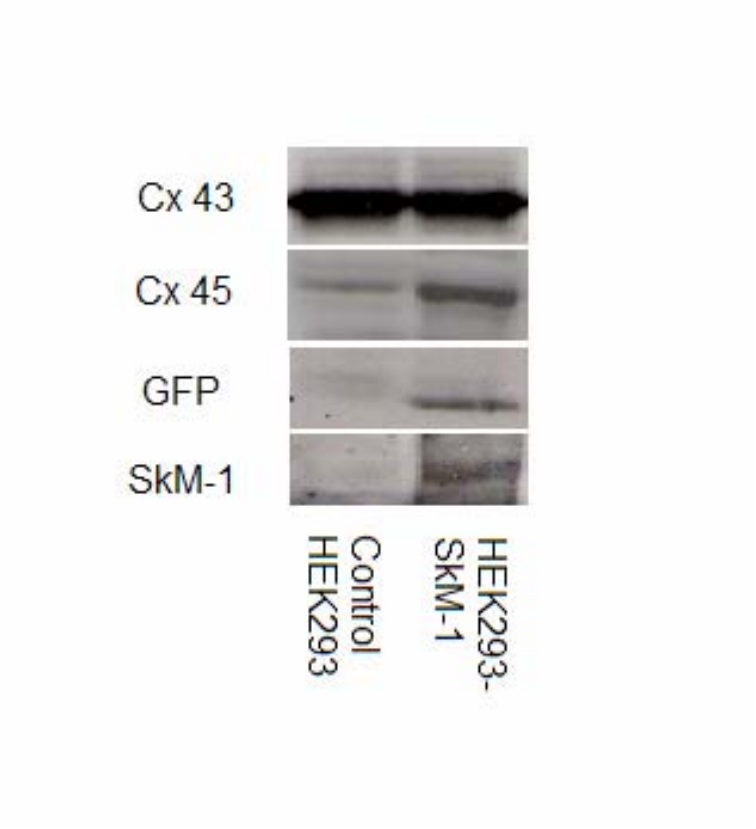

Fig 16. Western blot of non-transfected and transfected HEK293 cells. Both cell lines express Cx43 and Cx45. HEK293-SkM-1 cells express GFP and SkM-1.

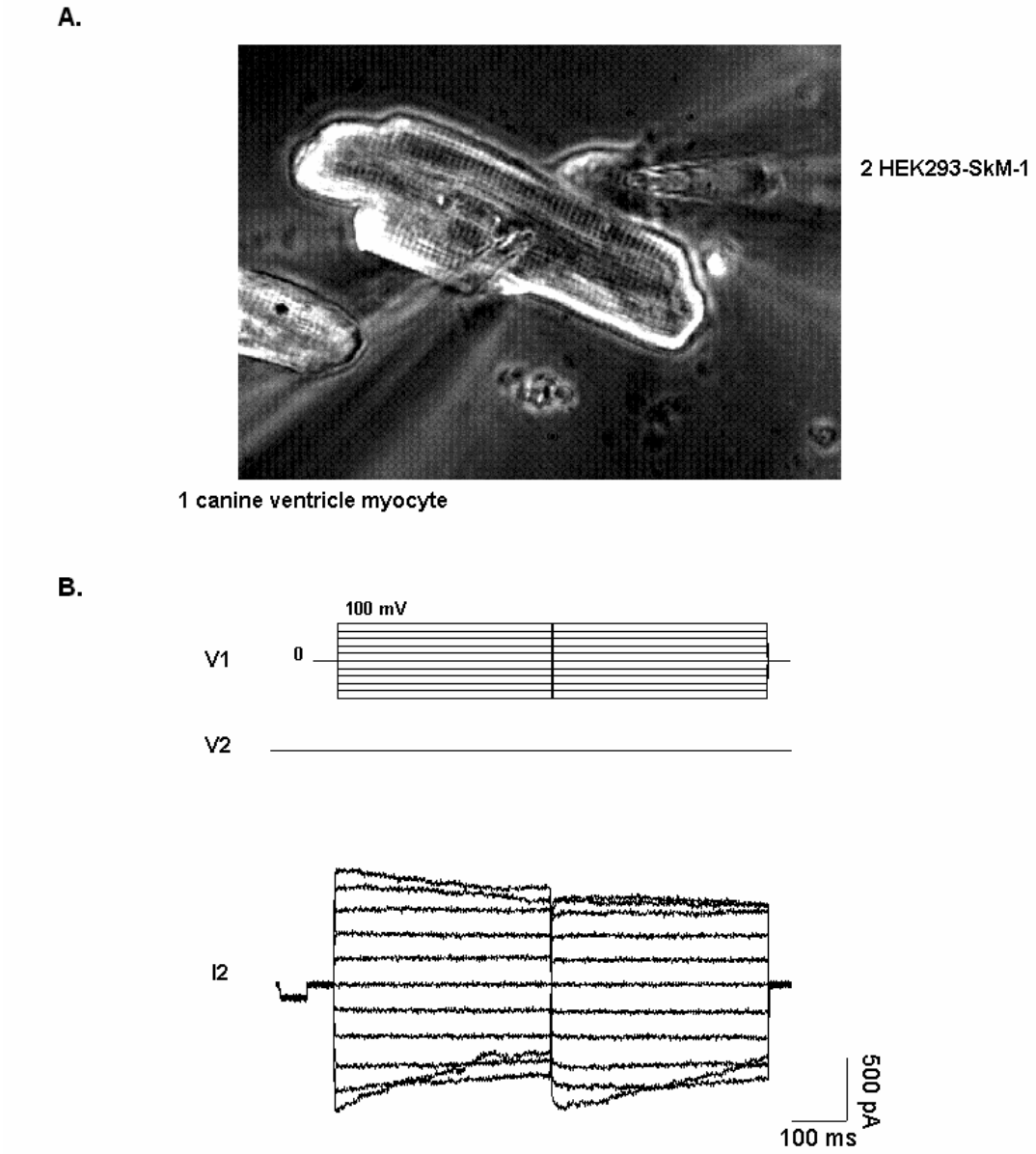

Fig 17. Electrical coupling of cultured adult canine myocyte and HEK293-SkM-1 cell. (A) Dual patch clamp of a myocyte-HEK293-SkM-1 cell pair. (B) The gap junction current between the cell pair. The conductance between the two cells was about 9 nS.

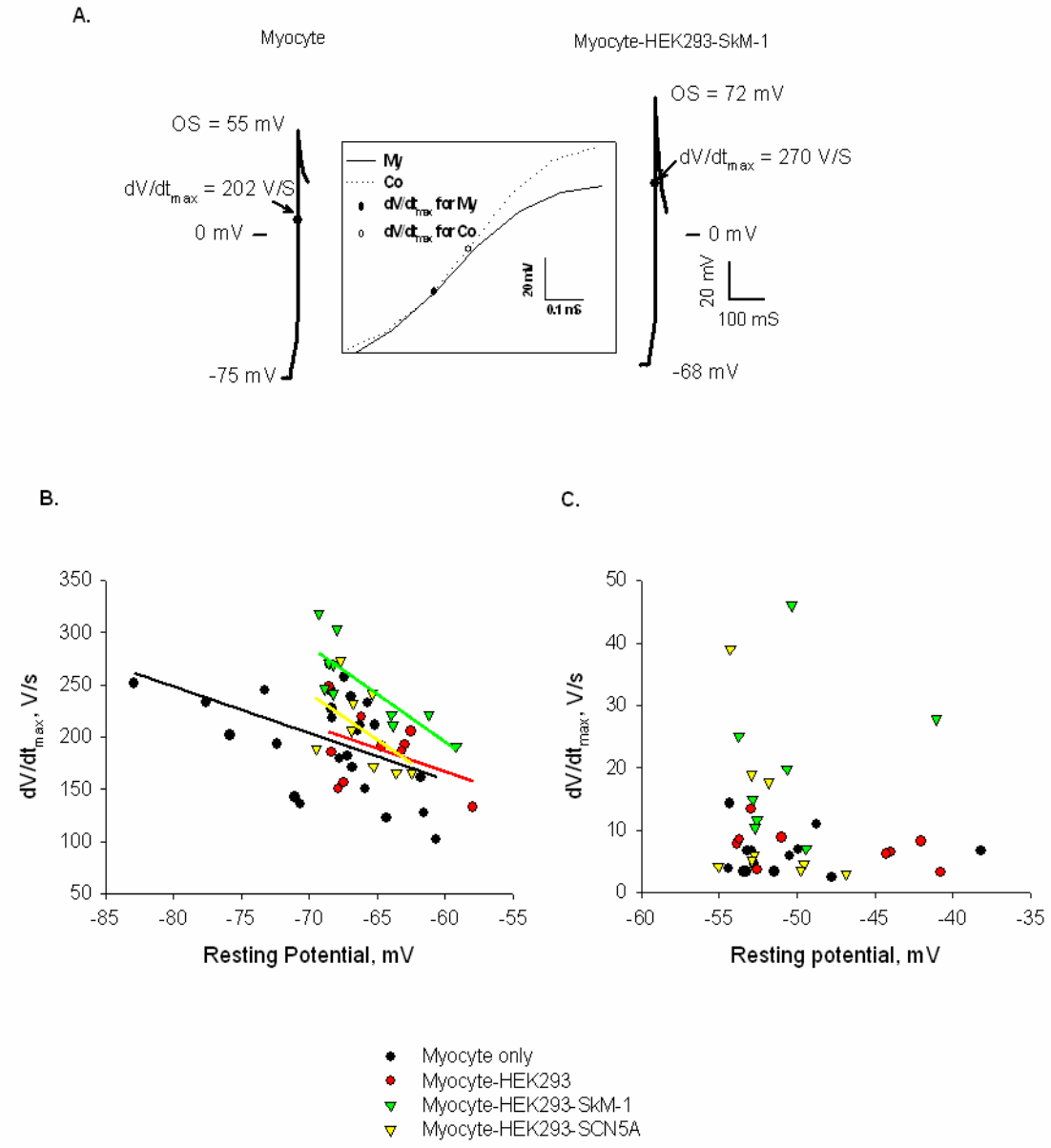
A.
Myocyte
Myocyte-HEK293-SkM-1
OS = 55 mV
dV/dtmax = 202 V/S
0 mV
-75 mV
My
Co
dV/dtmax for My
dV/dtmax for Co
20 mV
0.1 mS
OS = 72 mV
dV/dtmax = 270 V/S
0 mV
20 mV
100 mS
-68 mV
B.
C.
dV/dtmax, V/s
Resting Potential, mV
Resting potential, mV
Myocyte only
Myocyte-HEK293
Myocyte-HEK293-SkM-1
Myocyte-HEK293-SCN5A

Figure 18. Effect of expression SkM-1 on dV/dt_{max} of the action potential. (A). Action potential upstrokes generated in a cultured myocyte and a myocyte cocultured and coupled to a HEK293 cell expressing SkM-1. The resting potential is less negative but the dV/dt_{max} is greater and the overshoot is more positive in the myocyte coupled to the HEK-SkM-1 cell. The inset shows the dV/dt_{max} points of the two APs. **My**, myocyte only; **Co**, cocultured myocyte. **(B,C)** dV/dt_{max} vs. resting potential of four different culture conditions in normal K and high K solution, respectively. Data of normal K solution were fitted by linear regression:
Myocyte only: f = - 4.47x - 109.09, R = 0.4780
Myocyte-HEK293: f = -4.45x - 100.18, R = 0.4139
Myocyte-HEK293-SkM-1: f = -9.17x - 355.14, R = 0.8106
Myocyte-HEK293-SCN5A: f = -8.85x - 377.13, R = 0.5001

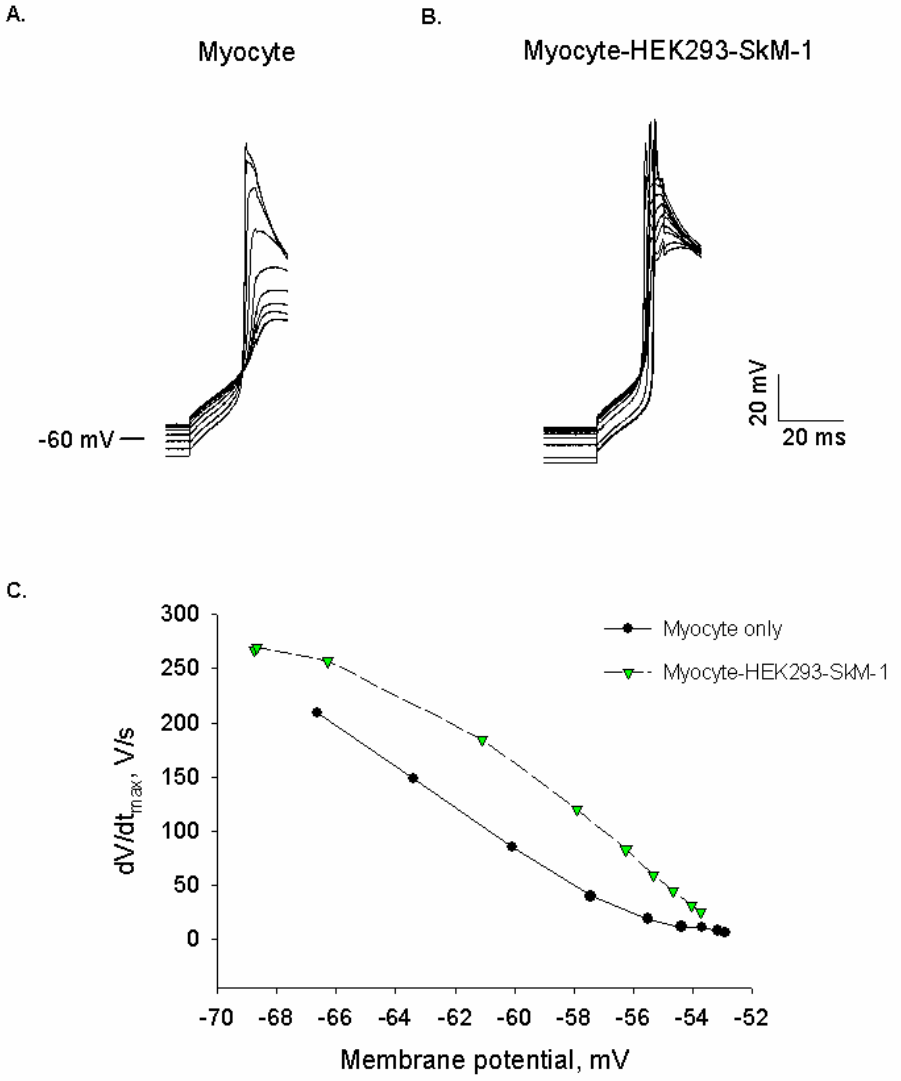

Figure 19. Change in dV/dt_{max} with resting potential. (A,B) The change in the upstroke velocity of the AP with perfusion of 10mM K^+ solution in a single myocyte and a myocyte coupled with a HEK293-SkM-1 cell. **(C)** dV/dt_{max} vs. membrane potential during perfusion of 10mM K^+ solution.

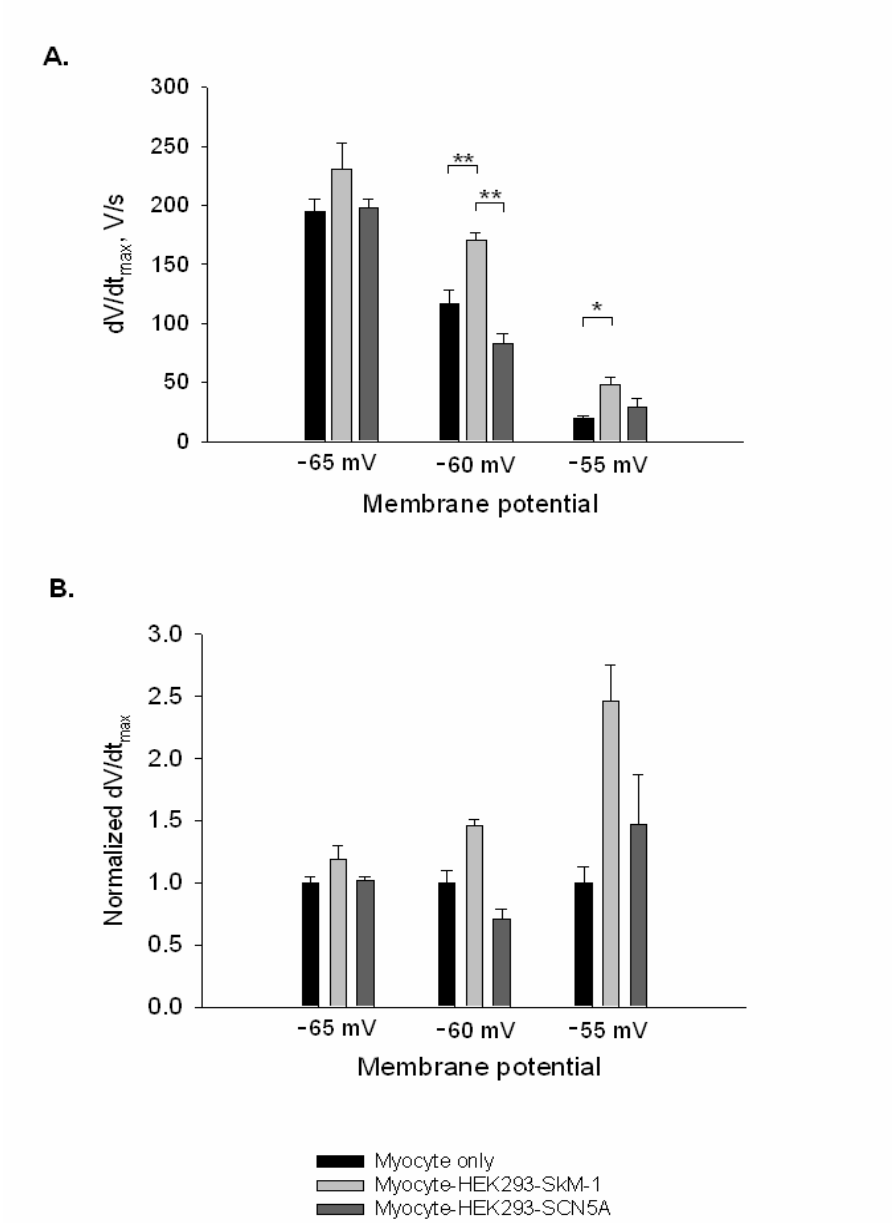

Figure 20. Comparison of dV/dt_{max} at -65, -60 and -55 mV. (A) dV/dtmax of three different cultures (mean±SE, n = 7, 5, 5 for myocyte, myocyte-HEK293-SCN5A, and myocyte-HEK293-SkM-1, respectively; ** P<0.001, * P<=0.002, ANOVA test). (B) Data were normalized to the mean value of the single myocyte at each potential.

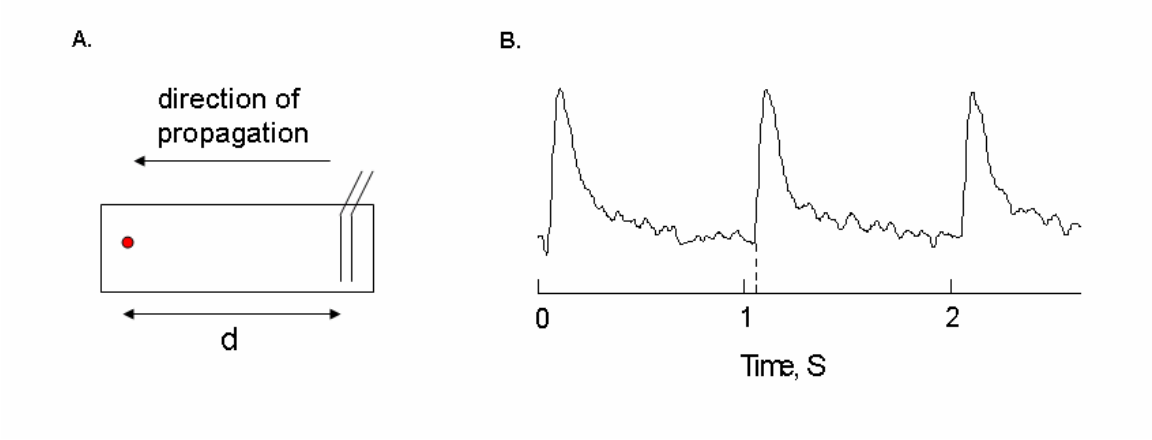

Figure 21. Measurement of conduction velocity. (A) A parallel Pt electrode is placed at one edge of the rectangular scaffold, and the recording site is shown as the red circle. d, the distance between the electrode and the recording site. (B). An example of fluorescence signal at the recording site with a 1Hz pacing frequency. The lag time (Δt) was estimated as the distance between the tick (stimulation point) and the dashed line (start of the signal). $CV = d / \Delta t$.

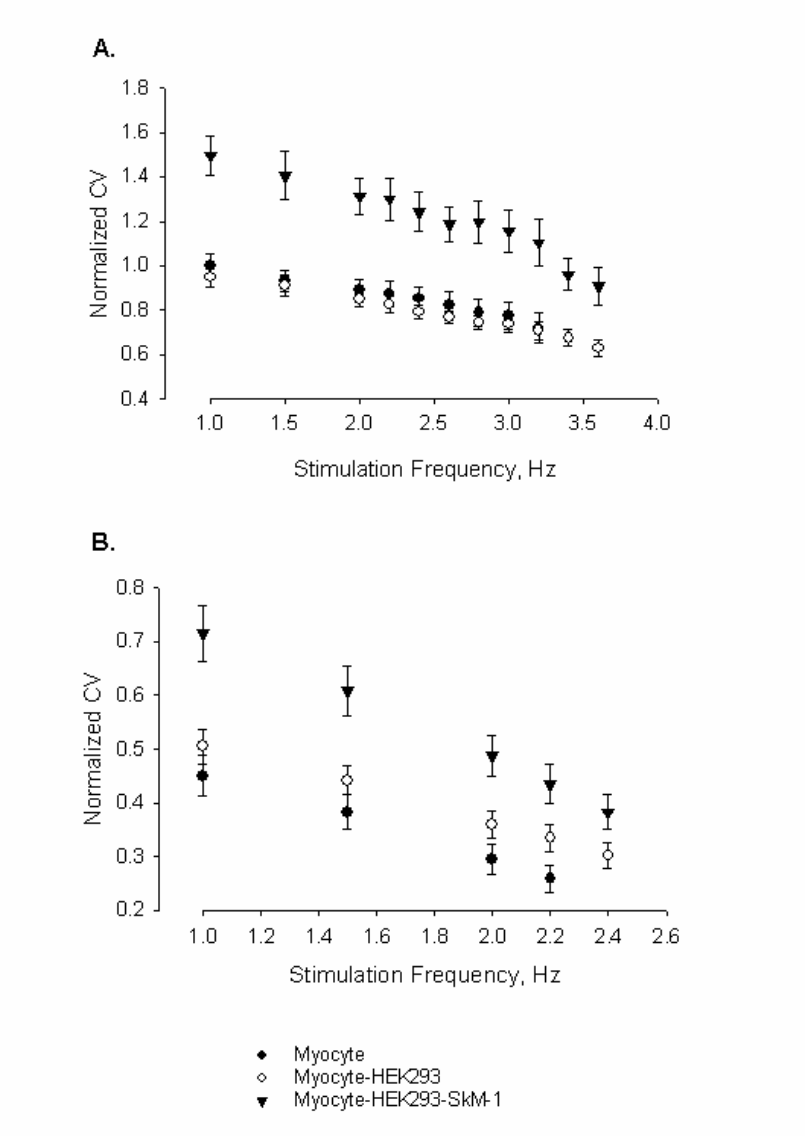

Figure 22. Effect of expression of SkM-1 on conduction velocity (CV) of APs of *in vitro* cardiac cultures in normal K (5.4 mM) (A) and high K (10.4 mM) (B) Tyrode's solutions at various stimulation frequencies. The data were normalized to the average CV values of control myocytes in normal Tyrode's solution at 1Hz for each experiment (mean±SE, n = 10, 12, 11 for myocyte, myocyte-HEK293, and myocyte-HEK293-SkM-1, respectively).

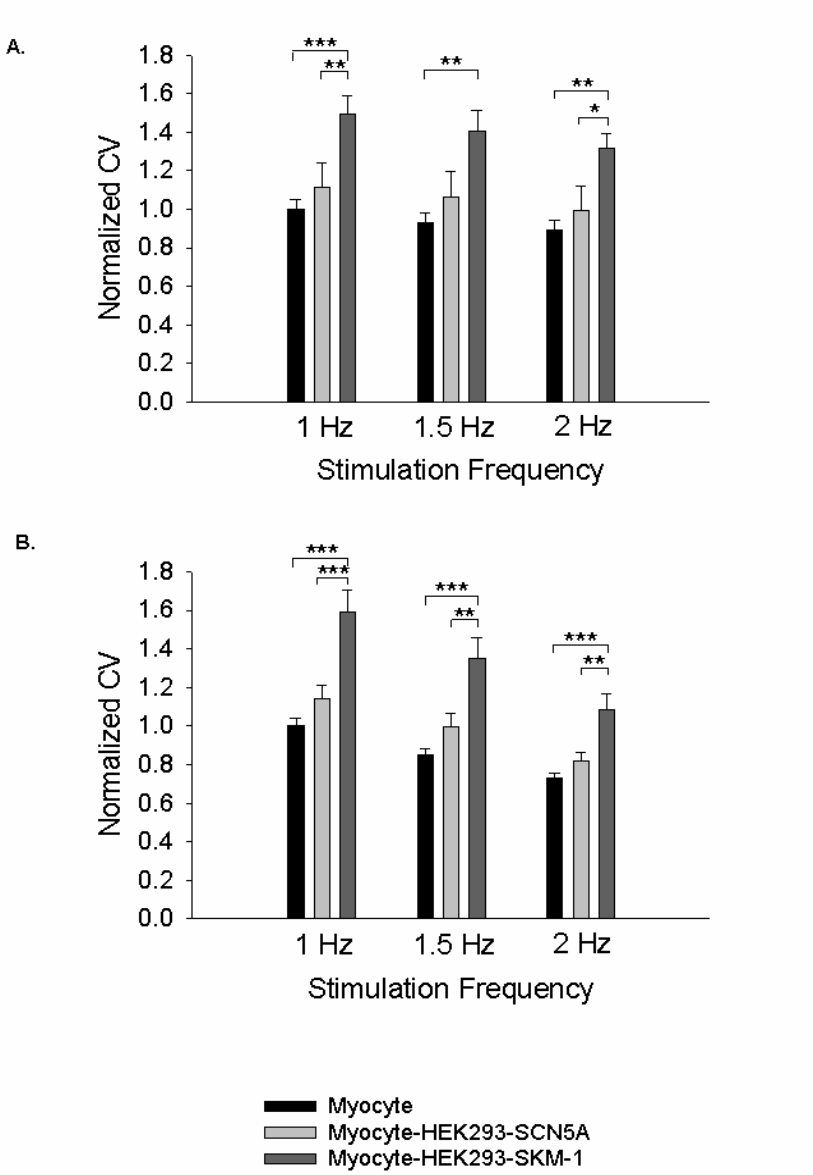

Figure 23. Comparison of CV between SkM-1 and SCN5A at 1, 1.5 and 2 Hz.

Data were normalized to the mean CV values of control myocytes in normal Tyrode's **(A)** or in high K solution **(B)**, respectively. (mean±SE, n = 10, 11, 10 for myocyte, myocyte-HEK293-SkM-1, and myocyte-HEK293-SCN5A, respectively; *** P=<0.001, ** P<0.01, * P<0.025, ANOVA test)

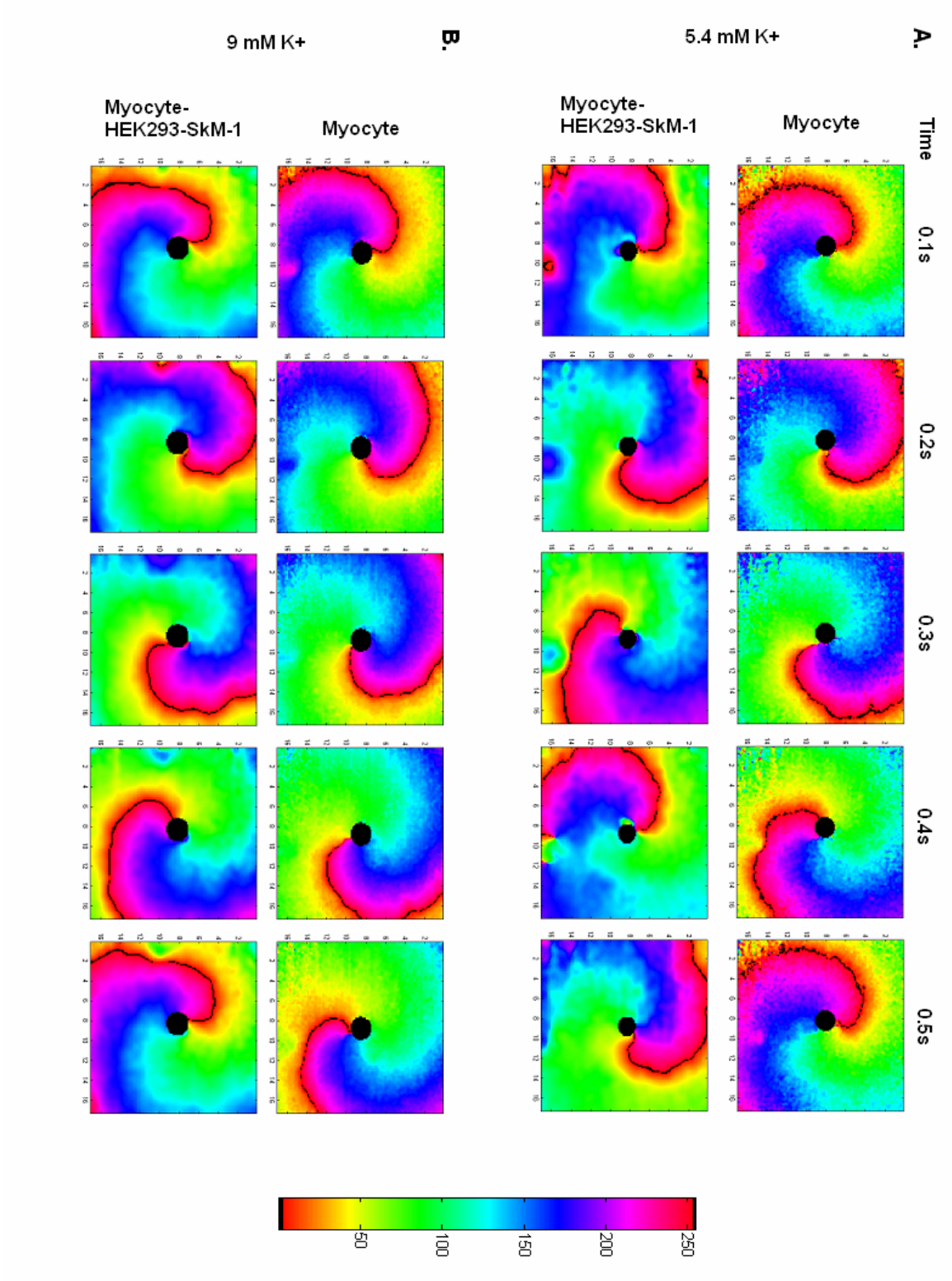
A.
5.4 mM K+
Myocyte-
HEK293-SkM-1
Myocyte
Time
0.1s
0.2s
0.3s
0.4s
0.5s
B.
9 mM K+
Myocyte-
HEK293-SkM-1
Myocyte
50
100
150
200
250

Figure 24. Phase graphs of induced re-entrant propagation. Phase movies were generated in Metlab software from macroscopic optical mapping data. Color bar shows the fluorescence intensity of Ca^{2+} signal. The black line shows the front head of the propagation. Frames were analyzed every 0.1s to show the propagation speed. (A) Examples of a myocyte only sample and a myocyte-HEK293-SkM-1 sample in 5.4 mM K^+ Tyrodes. (B) Examples of a myocyte only sample and a myocyte-HEK293-SkM-1 sample in 10.4 mM K^+ Tyrodes.

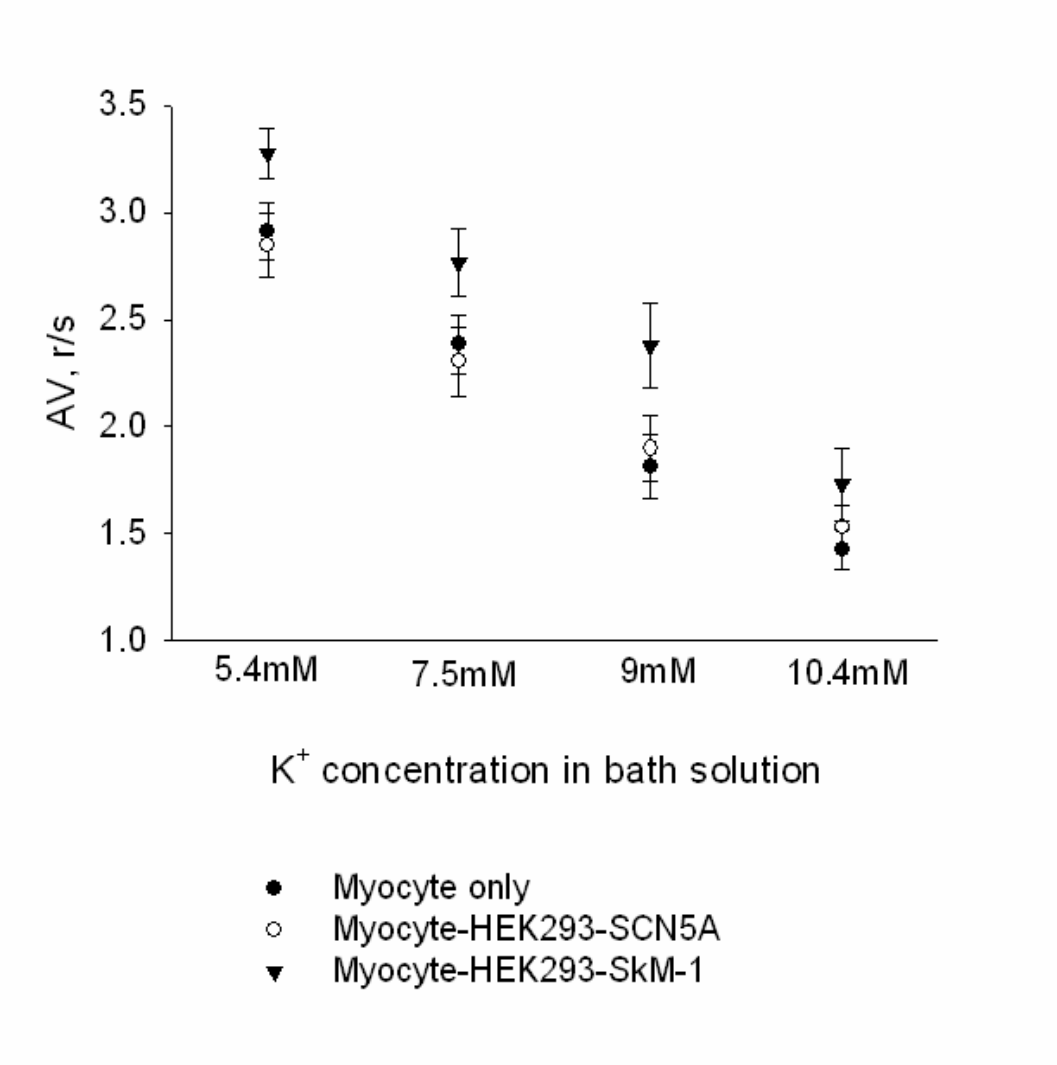

Figure 25. Effect of expression of SkM-1 on angular velocity (AV) of APs propagation of induced re-entry at different K^+ concentrations. Data are expressed as mean±SE, n = 7 for each group. (r/s: round/sec). Two way ANOVA (Holm-Sidak) test showed a significant difference between Myocyte only and Myocyte-HEK293-SkM-1 ($P<0.001$), and between Myocyte-HEK293-SCN5A and Myocyte-HEK293-SkM-1 ($P<0.001$), but no difference between Myocyte only and Myocyte-HEK293=SCN5A.

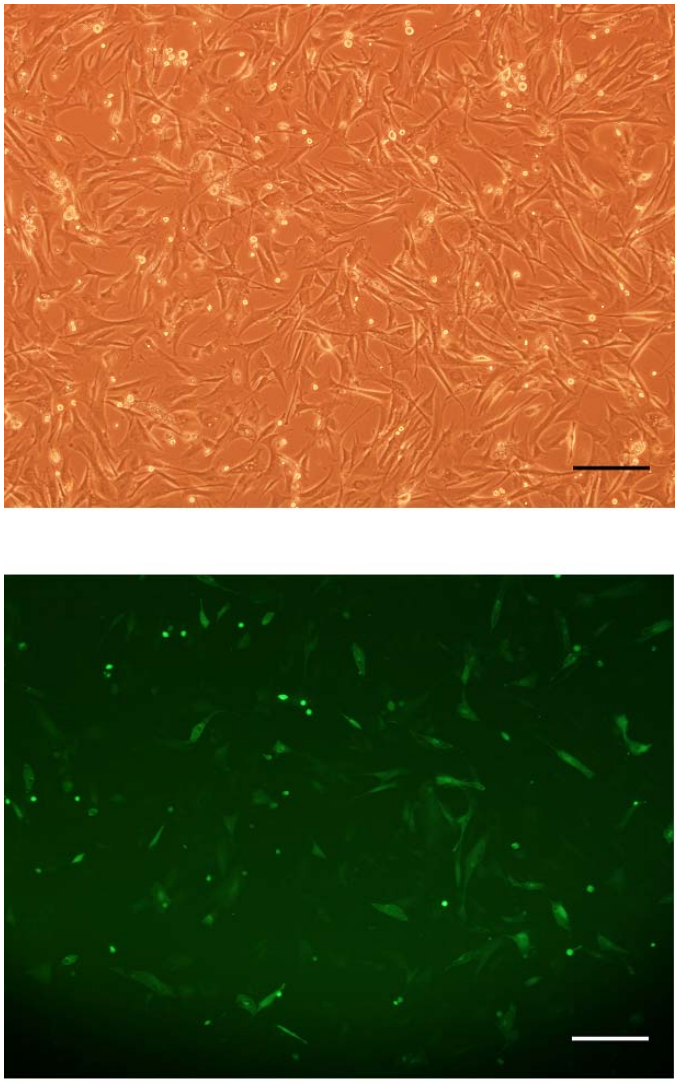

Figure 26. Expression of GFP in cMSC-SkM-1 cells. The upper panel shows phase contrast image of cMSC-SkM-1 cells. The lower panel shows GFP expression. Fluorescence was detected 24 hours after trasfection. (Scale bar, 200 μm)

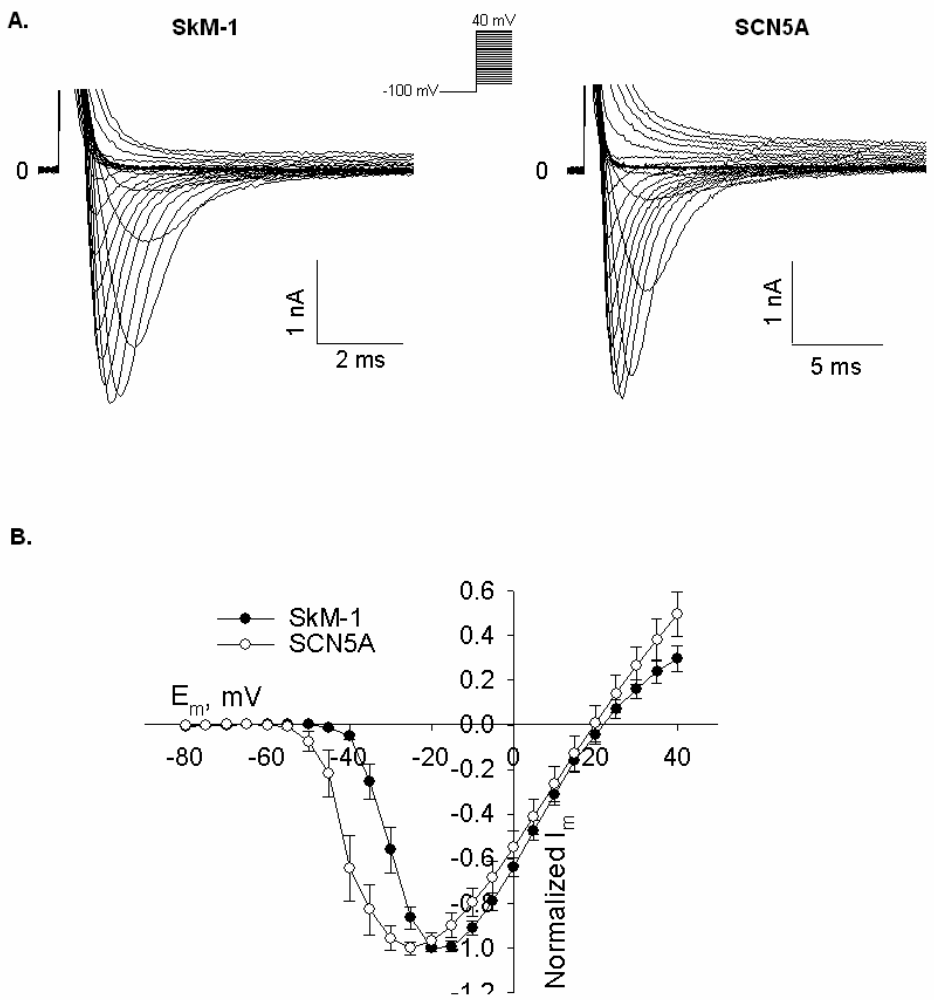

Figure 27. Activation of SkM-1 and SCN5A in cMSCs. (A) Expression of SkM-1 or SCN5A in cMSCs. Na^+ currents were recorded in low Na^+ (15 mM) Tyrode's solution at room temperature. (B) Current-voltage relationship of SkM-1 (n=8) and SCN5A (n=8) in cMSCs. Cells were held at -100 mV and then pulsed to test potentials from -80 mV to +40 mV, with a 5 mV increment. Data are normalized to the maximum peak current (mean±SE). The peak current densities of the two channels were 38.52±4.74 (SkM-1) and 55.09±10.6 (SCN5A) pA/pF.

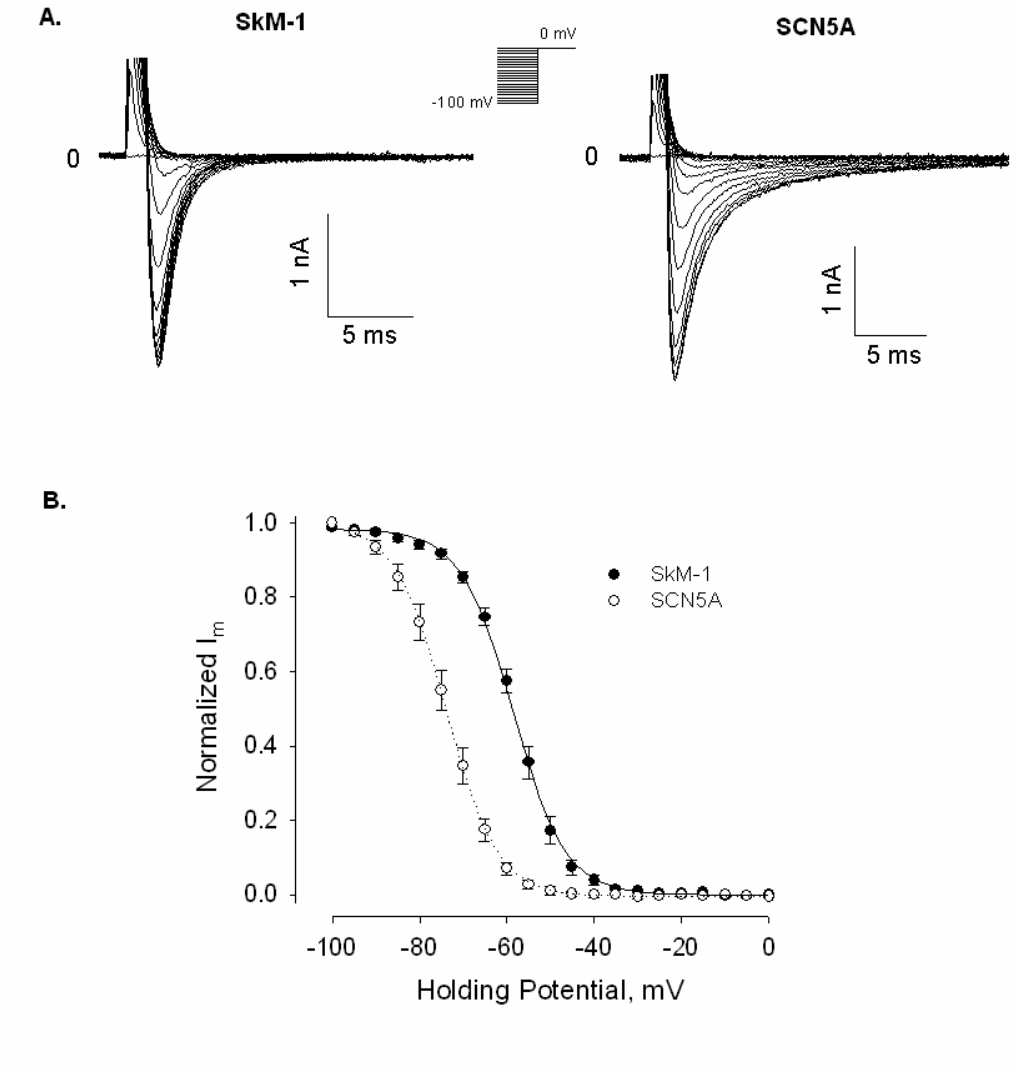

Figure 28. Inactivation of SkM-1 and SCN5A in cMSCs.
(A) Representative inactivation of SkM-1 and SCN5A currents in cMSCs. **(B)** Inactivation curve (the h_∞ curve) of SkM-1 (n=8) and SCN5A (n=8). Data are normalized to the maximum peak current and fit to the Boltzmann equation $f = \frac{1}{1+\exp[(Em-Vh)/K]}$, where V_h is the midpoint membrane potential and K is the slope factor (mean±SE).

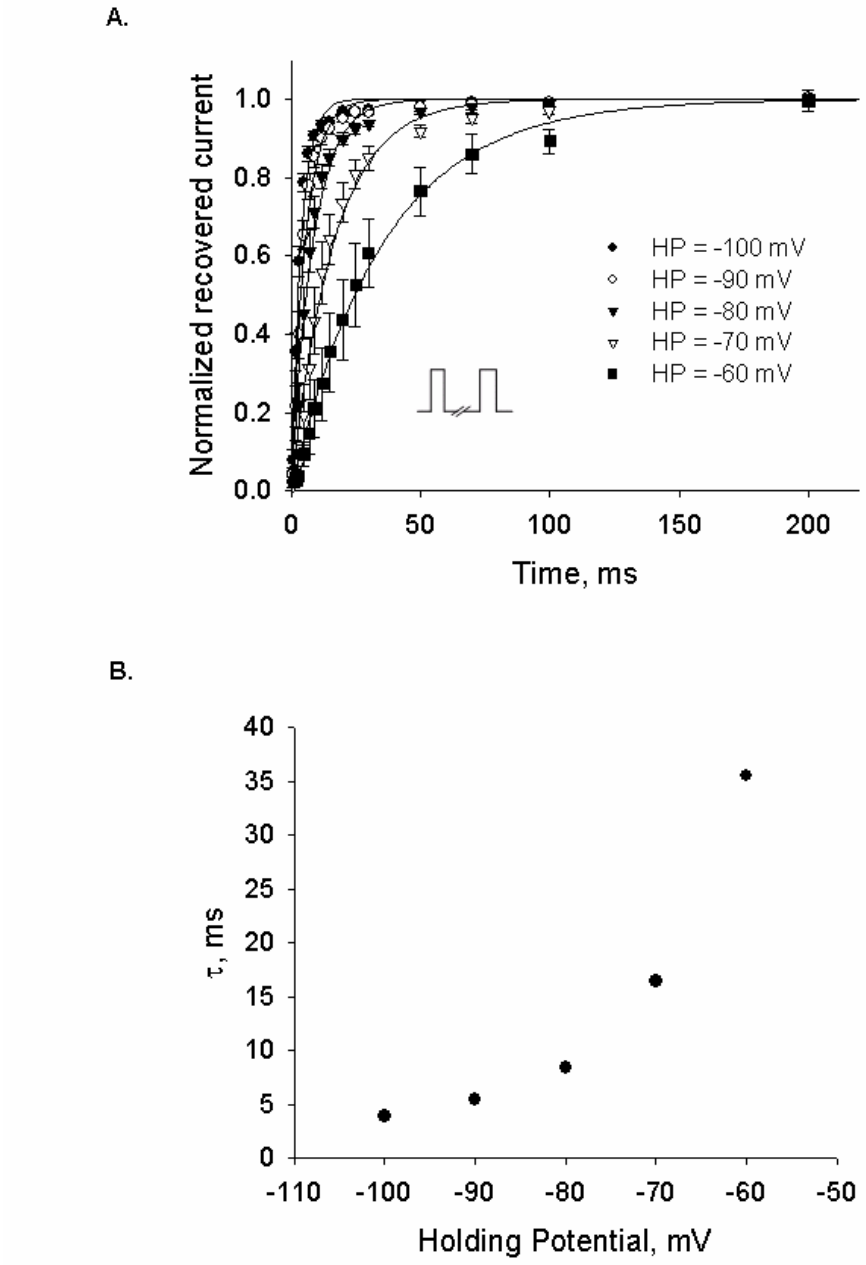

Figure 29. Recovery of SkM-1 in cMSCs. Data were normalized to the current amplitude of the first pulse (mean±SE, n = 8 for each holding potential) and curve fit to the equation $f = 1 - \exp(-t/\tau)$.

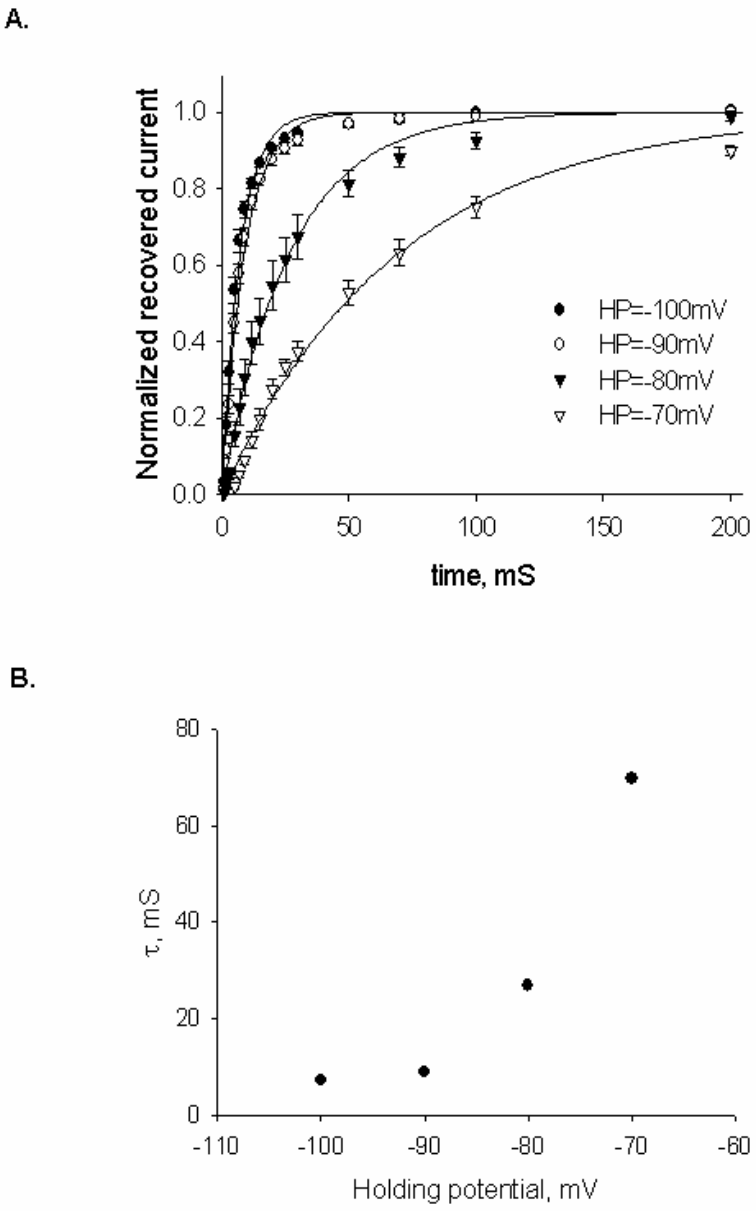

Figure 30. Recovery of SCN5A in cMSCs. Data were normalized to the current amplitude of the first pulse (mean ± SE, n = 8 for each holding potential) and curve fit to the equation $f = 1 - \exp(-t/\tau)$.

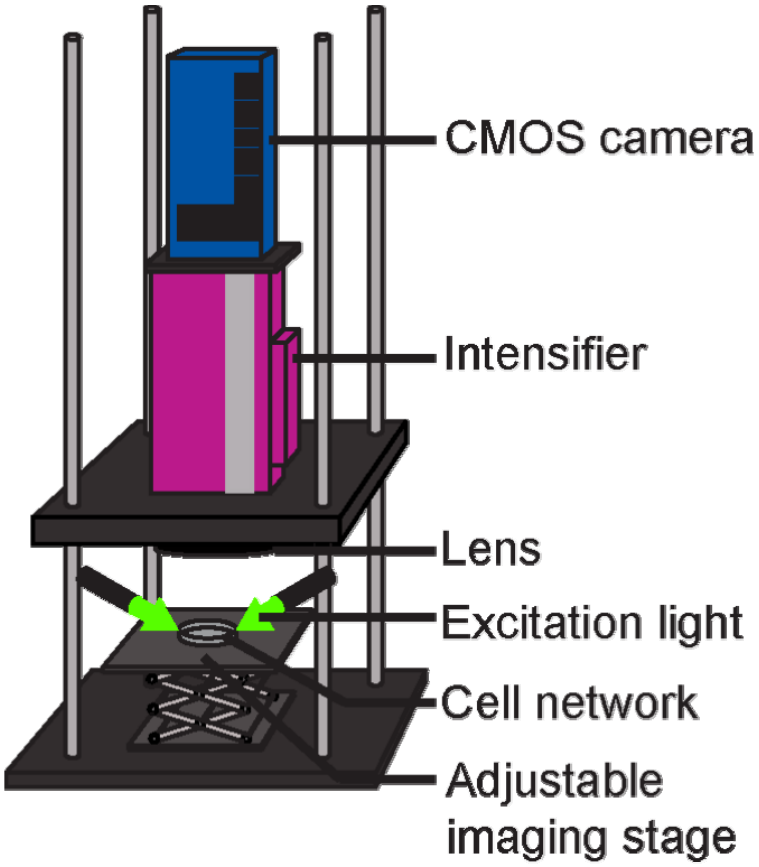

Figure 31. Macroscopic optical mapping setup. Image courtesy of L. Varghese.

Table 1. Conduction velocities of different cardiac tissues[85].

Tissue	Atria	AV Node	Bundle of His	Ventricles	Bundle Branches	Purkinje Fibers
CV (m/sec)	(0.1-0.3)	~0.05	~2	(0.1-0.3)	~2	3-5

Table 2. Mutations of SCN5A in arrhythmias.

	Syndrome	Mutation	Functional change
Loss of function	Brugada syndrome[86]	Truncation[87]	Non-functional protein
		T1620M in S3-S4 loop of domain IV[87]	Accelerated decay kinetics
		1795insD of the C terminal domain[88]	Inactivation shift to negative potential
	Conduction block	G514C in the I-II linker[89]	Activation shift to positive potential & enhanced inactivation rate
Gain of function	LQT 3[90]	DKPQ (deletion) in the III-IV linker[91]	Failure of fast inactivation
		R1644H or N1325S in the S4-S5 linker[92]	

Table 3. Comparison of the recovery time constants between SkM-1 and SCN5A in HEK293 cells.

	τ of SkM-1, mS	τ of SCN5A, mS
-100 mV	1.677	7.273
-90 mV	2.335	9.001
-80 mV	3.338	26.81
-70 mV	5.155	69.78
-60 mV	8.130	--
-50 mV	14.58	--

Table 4. Comparison of the recovery time constants between SkM-1 and SCN5A in cMSCs.

	τ of SkM-1, mS	τ of SCN5A, mS
-100 mV	3.9090	6.667
-90 mV	5.4580	12.441
-80 mV	8.4320	33.75
-70 mV	16.4360	101.46
-60 mV	35.5490	--

REFERENCES

1. Robbins, J. and G. W. Dorn, 2nd (2000). "Listening for hoof beats in heart beats." Nat Med **6**(9): 968-70.

2. Bigger, J. T. (1980). "Mechanisms and diagnosis of arrhythmias." In Bradunwald, Eugene "Heart disease: a textbook of cardiovascular medicine." Philadelphia, W.B. Saunders: 631.

3. Rohr, S. (2004). "Role of gap junctions in the propagation of the cardiac action potential." Cardiovasc Res **62**(2): 309-22.

4. Zara, A. (2000). "The cardiac action potential." In Rosen, M. R. and Zara, A. "An introduction to cardiac electrophysiology." Harwood academic publishers: 59.

5. Irisawa, H., H. F. Brown, et al. (1993). "Cardiac pacemaking in the sinoatrial node." Physiol Rev **73**(1): 197-227.

6. Scottish Intercollegiate Guidelines Network (SIGN). (2007) "Cardiac arrhythmias in coronary heart disease. A national clinical guideline." (SIGN publication; no. 94) Edinburgh (Scotland) Feb: 40.

7. Marcus, F. I., L. A. Cobb, et al. (1988). "Mechanism of death and prevalence of myocardial ischemic symptoms in the terminal event after acute myocardial infarction." Am J Cardiol **61**(1): 8-15.

8. Welsh, M. J. and T. Hoshi (1995). "Molecular cardiology. Ion channels lose the rhythm." Nature **376**(6542): 640.

9. Ackerman, M. J. (1998). "The long QT syndrome: ion channel diseases of the heart." Mayo Clin Proc **73**(3): 250-69.

10. Spear, J. F. and E. N. Moore (1982). "Mechanisms of cardiac arrhythmias." Annu Rev Physiol **44**: 485-97.

11. McPherson, C.A. and L.E. Rosenfeld (1992). "Heart rhythm disorders." In Yale University School of Medicine "Heart book":195.

12. Allessie, M. A., F. I. Bonke, et al. (1976). "Circus movement in rabbit atrial muscle as a mechanism of tachycardia. II. The role of nonuniform recovery of excitability in the occurrence of unidirectional block, as studied with multiple microelectrodes." Circ Res **39**(2): 168-77.

13. Roden, D. M., R. Lazzara, et al. (1996). "Multiple mechanisms in the long-QT syndrome. Current knowledge, gaps, and future directions. The SADS Foundation Task Force on LQTS." Circulation **94**(8): 1996-2012.

14. Roden, D. M. (1998). "Mechanisms and management of proarrhythmia." Am J Cardiol **82**(4A): 49I-57I.

15. Curran, M. E., I. Splawski, et al. (1995). "A molecular basis for cardiac arrhythmia: HERG mutations cause long QT syndrome." Cell **80**(5): 795-803.

16. Roden, D. M. and A. L. George, Jr. (1996). "The cardiac ion channels: relevance to management of arrhythmias." Annu Rev Med **47**: 135-48.

17. Roden, D. M., J. R. Balser, et al. (2002). "Cardiac ion channels." Annu Rev Physiol **64**: 431-75.

18. Gellens, M. E., A. L. George, Jr., et al. (1992). "Primary structure and functional expression of the human cardiac tetrodotoxin-insensitive voltage-dependent sodium channel." Proc Natl Acad Sci U S A **89**(2): 554-8.

19. Hodgkin, A. L. and A. F. Huxley (1952). "A quantitative description of membrane current and its application to conduction and excitation in nerve." J Physiol **117**(4): 500-44.

20. Spear, J. F., E. L. Michelson, et al. (1983). "Cellular electrophysiologic characteristics of chronically infarcted myocardium in dogs susceptible to sustained ventricular tachyarrhythmias." J Am Coll Cardiol **1**(4): 1099-110.

21. Lue, W. M. and P. A. Boyden (1992). "Abnormal electrical properties of myocytes from chronically infarcted canine heart. Alterations in Vmax and the transient outward current." Circulation **85**(3): 1175-88.

22. Pinto, J. M. and P. A. Boyden (1999). "Electrical remodeling in ischemia and infarction." Cardiovasc Res **42**(2): 284-97.

23. Baba, S., W. Dun, et al. (2005). "Remodeling in cells from different regions of the reentrant circuit during ventricular tachycardia." Circulation **112**(16): 2386-96.

24. Zipes, D. P. and H. J. Wellens (1998). "Sudden cardiac death." Circulation **98**(21): 2334-51.

25. McDonald, A. J., A. J. Pelletier, et al. (2008). "Increasing US emergency department visit rates and subsequent hospital admissions for atrial fibrillation from 1993 to 2004." Ann Emerg Med **51**(1): 58-65.

26. Danilo, P. et al. (2005). "Gene and cell therapy for sinus and AV nodal dysfunction." In "New Arrhythmia Technologies." P.J. Wang (ed): 54.

27. Vaughan Williams, E. M. (1992). "Classifying antiarrhythmic actions: by facts or speculation." J Clin Pharmacol **32**(11): 964-77.
28. Spinelli, W. (2000). "Pharmacological modulation of cardiac electrophysiologic properties." In Rosen, M. R. and Zara, A. "An introduction to cardiac electrophysiology." Harwood academic publishers: 174.

29. Knight, B. P., R. Weiss, et al. (1997). "Cost comparison of radiofrequency modification and ablation of the atrioventricular junction in patients with chronic atrial fibrillation." Circulation **96**(5): 1532-6.

30. Parsonnet, V., A. D. Bernstein, et al. (1989). "Pacemaker-implantation complication rates: an analysis of some contributing factors." J Am Coll Cardiol **13**(4): 917-21.

31. Francis, J. (2002). "Electromagnetic interference in implantable rhythm devices--the Indian scenario." Indian Pacing Electrophysiol J **2**(3): 64-5.

32. From Wikipedia. "Gene therapy." http://en.wikipedia.org/wiki/Gene_therapy.

33. Donahue, J. K., A. W. Heldman, et al. (2000). "Focal modification of electrical conduction in the heart by viral gene transfer." Nat Med **6**(12): 1395-8.

34. Qu, J., A. N. Plotnikov, et al. (2003). "Expression and function of a biological pacemaker in canine heart." Circulation **107**(8): 1106-9.

35. Orlic, D., J. Kajstura, et al. (2001). "Bone marrow cells regenerate infarcted myocardium." Nature **410**(6829): 701-5.

36. Orlic, D., J. Kajstura, et al. (2001). "Mobilized bone marrow cells repair the infarcted heart, improving function and survival." Proc Natl Acad Sci U S A **98**(18): 10344-9.

37. Pittenger, M. F. and B. J. Martin (2004). "Mesenchymal stem cells and their potential as cardiac therapeutics." Circ Res **95**(1): 9-20.

38. Pittenger, M.F. and Marshak, D.R. (2001). "Mesenchymal stem cells of human adult bone marrow." Marshak, D.R., Gardner, D.K., and Gottlieb, D. eds. (Cold Spring Harbor, New York: Cold Spring Harbor Laboratory Press). 349-374.

39. Pittenger, M. F., A. M. Mackay, et al. (1999). "Multilineage potential of adult human mesenchymal stem cells." Science **284**(5411): 143-7.

40. Valiunas, V., S. Doronin, et al. (2004). "Human mesenchymal stem cells make cardiac connexins and form functional gap junctions." J Physiol **555**(Pt 3): 617-26.

41. Liechty, K. W., T. C. MacKenzie, et al. (2000). "Human mesenchymal stem cells engraft and demonstrate site-specific differentiation after in utero transplantation in sheep." Nat Med **6**(11): 1282-6.

42. Augello, A., R. Tasso, et al. (2007). "Cell therapy using allogeneic bone marrow mesenchymal stem cells prevents tissue damage in collagen-induced arthritis." Arthritis Rheum **56**(4): 1175-86.

43. Amado, L. C., A. P. Saliaris, et al. (2005). "Cardiac repair with intramyocardial injection of allogeneic mesenchymal stem cells after myocardial infarction." Proc Natl Acad Sci U S A **102**(32): 11474-9.

44. Potapova, I., A. Plotnikov, et al. (2004). "Human mesenchymal stem cells as a gene delivery system to create cardiac pacemakers." Circ Res **94**(7): 952-9.

45. Nuss, H. B., G. F. Tomaselli, et al. (1995). "Cardiac sodium channels (hH1) are intrinsically more sensitive to block by lidocaine than are skeletal muscle (μ1) channels." J Gen Physiol **106**(6): 1193-209.

46. Wang, D. W., A. L. George, Jr., et al. (1996). "Comparison of heterologously expressed human cardiac and skeletal muscle sodium channels." Biophys J **70**(1): 238-45.

47. Zygmunt, A. C. (1994). "Intracellular calcium activates a chloride current in canine ventricular myocytes." Am J Physiol **267**(5 Pt 2): H1984-95

48. Entcheva, E., S. N. Lu, et al. (2000). "Contact fluorescence imaging of reentry in monolayers of cultured neonatal rat ventricular myocytes." J Cardiovasc Electrophysiol **11**(6): 665-76.

49. Chung, C. Y., H. Bien, et al. (2007). "The role of cardiac tissue alignment in modulating electrical function." J Cardiovasc Electrophysiol **18**(12): 1323-9.

50. Tolkacheva, E. G., D. G. Schaeffer, et al. (2003). "Condition for alternans and stability of the 1:1 response pattern in a "memory" model of paced cardiac dynamics." Phys Rev E Stat Nonlin Soft Matter Phys **67**(3 Pt 1): 031904.

51. Entcheva, E. and H. Bien (2006). "Macroscopic optical mapping of excitation in cardiac cell networks with ultra-high spatiotemporal resolution." Prog Biophys Mol Biol **92**(2): 232-57.

52. Trimmer, J. S., S. S. Cooperman, et al. (1989). "Primary structure and functional expression of a mammalian skeletal muscle sodium channel." Neuron **3**(1): 33-49.

53. Goldin, A. L. (2001). "Resurgence of sodium channel research." Annu Rev Physiol **63**: 871-94.

54. Baba, S., W. Dun, et al. (2005). "Remodeling in cells from different regions of the reentrant circuit during ventricular tachycardia." Circulation **112**(16): 2386-96.

55. Baba, S., W. Dun, et al. (2006). "Sodium current function in adult and aged canine atrial cells." Am J Physiol Heart Circ Physiol **291**(2): H756-61.

56. Hayward, L. J., R. H. Brown, Jr., et al. (1996). "Inactivation defects caused by myotonia-associated mutations in the sodium channel III-IV linker." J Gen Physiol **107**(5): 559-76.

57. Graham, F. L., J. Smiley, et al. (1977). "Characteristics of a human cell line transformed by DNA from human adenovirus type 5." J Gen Virol **36**(1): 59-74.

58. Toyofuku, T., M. Yabuki, et al. (1998). "Intercellular calcium signaling via gap junction in connexin-43-transfected cells." J Biol Chem **273**(3): 1519-28.

59. John, S. A., R. Kondo, et al. (1999). "Connexin-43 hemichannels opened by metabolic inhibition." J Biol Chem **274**(1): 236-40.

60. Kanter, H. L., J. E. Saffitz, et al. (1992). "Cardiac myocytes express multiple gap junction proteins." Circ Res **70**(2): 438-44.

61. Athias, P., and A. Grynberg. (1987). "Electrophysiological studies on heart cells in culture." In "The Heart CelZ in Culture." Boca Raton, FL: CRC, vol. I: 125-158.

62. Mandel, G. (1992). "Tissue-specific expression of the voltage-sensitive sodium channel." J Membr Biol **125**(3): 193-205.

63. O'Leary, M. E. (1998). "Characterization of the isoform-specific differences in the gating of neuronal and muscle sodium channels." Can J Physiol Pharmacol **76**(10-11): 1041-50.

64. Jonas, P. (1989). "Temperature dependence of gating current in myelinated nerve fibers." J Membr Biol **112**(3): 277-89.

65. Ruff, R. L. (1999). "Effects of temperature on slow and fast inactivation of rat skeletal muscle Na(+) channels." Am J Physiol **277**(5 Pt 1): C937-47.

66. Featherstone, D. E., J. E. Richmond, et al. (1996). "Interaction between fast and slow inactivation in Skm1 sodium channels." Biophys J **71**(6): 3098-109.

67. Goldin, A. L. (2003). "Mechanisms of sodium channel inactivation." Curr Opin Neurobiol **13**(3): 284-90.

68. Lau, D. H., C. Clausen, et al. (2008) Epicardial border zone overexpression of skeletal muscle sodium channel, SkM1, normalized activation, preserves conduction and suppresses ventricular arrhythmia: an *in silico, in vivo, in vitro* study. Circulation (Accepted)

69. Deschenes, I., E. Trottier, et al. (2001). "Implication of the C-terminal region of the alpha-subunit of voltage-gated sodium channels in fast inactivation." J Membr Biol **183**(2): 103-14.

70. Vilin, Y. Y., E. Fujimoto, et al. (2001). "A single residue differentiates between human cardiac and skeletal muscle Na+ channel slow inactivation." Biophys J **80**(5): 2221-30.

71. Hayward, L. J., R. H. Brown, Jr., et al. (1996). "Inactivation defects caused by myotonia-associated mutations in the sodium channel III-IV linker." J Gen Physiol **107**(5): 559-76.

72. "Gene Therapy. Human Genome Project Information." Oak Ridge National Laboratory. www.ornl.gov

73. Woods, N. B., V. Bottero, et al. (2006). "Gene therapy: therapeutic gene causing lymphoma." Nature **440**(7088): 1123.

74. Lo, C. W. (2000). "Role of gap junctions in cardiac conduction and development: insights from the connexin knockout mice." Circ Res **87**(5): 346-8.

75. Van Kempen, M. J., C. Fromaget, et al. (1991). "Spatial distribution of connexin43, the major cardiac gap junction protein, in the developing and adult rat heart." Circ Res **68**(6): 1638-51.

76. Gourdie, R. G. and C. W. Lo. (2000). "Cx43 ($_1$) gap junctions in cardiac development and disease." Curr Top Membr **49**: 581–602.

77. Beblo, D. A. and R. D. Veenstra (1997). "Monovalent cation permeation through the connexin40 gap junction channel. Cs, Rb, K, Na, Li, TEA, TMA, TBA, and effects of anions Br, Cl, F, acetate, aspartate, glutamate, and NO3." J Gen Physiol **109**(4): 509-22.

78. Swenson, K. I., J. R. Jordan, et al. (1989). "Formation of gap junctions by expression of connexins in Xenopus oocyte pairs." Cell **57**(1): 145-55.

79. Werner, R., E. Levine, et al. (1989). "Formation of hybrid cell-cell channels." Proc Natl Acad Sci U S A **86**(14): 5380-4.

80. White, T. W., D. L. Paul, et al. (1995). "Functional analysis of selective interactions among rodent connexins." Mol Biol Cell **6**(4): 459-70.

81. Brink, P. R., K. Cronin, et al. (1997). "Evidence for heteromeric gap junction channels formed from rat connexin43 and human connexin37." Am J Physiol **273**(4 Pt 1): C1386-96.

82. Schackow, T. E., R. S. Decker, et al. (1995). "Electrophysiology of adult cat cardiac ventricular myocytes: changes during primary culture." Am J Physiol **268**(4 Pt 1): C1002-17.

83. O'Reilly, J. P., S. Y. Wang, et al. (1999). "Comparison of slow inactivation in human heart and rat skeletal muscle Na+ channel chimaeras." J Physiol **515 (Pt 1)**: 61-73.

84. Protas, L., W. Dun, et al. (2008). "Expression of skeletal but not cardiac Na^+ channel isoform preserves normal conduction in a depolarized cardiac syncytium." Cadiovasc Res (Accepted)

85. Levick, J. R. (1995) "Initiation of heart beat and nervous control." In "An introduction to cardiovascular physiology." Second edition. Oxford, Butterworth-Heinemann Ltd.: 44

86. Brugada, P. and J. Brugada (1992). "Right bundle branch block, persistent ST segment elevation and sudden cardiac death: a distinct clinical and electrocardiographic syndrome. A multicenter report." J Am Coll Cardiol **20**(6): 1391-6.

87. Chen, Q., G. E. Kirsch, et al. (1998). "Genetic basis and molecular mechanism for idiopathic ventricular fibrillation." Nature **392**(6673): 293-6.

88. Bezzina, C., M. W. Veldkamp, et al. (1999). "A single Na(+) channel mutation causing both long-QT and Brugada syndromes." Circ Res **85**(12): 1206-13.

89. Tan, H. L., M. T. Bink-Boelkens, et al. (2001). "A sodium-channel mutation causes isolated cardiac conduction disease." Nature **409**(6823): 1043-7.

90. Wang, Q., J. Shen, et al. (1995). "SCN5A mutations associated with an inherited cardiac arrhythmia, long QT syndrome." Cell **80**(5): 805-11.

91. Nuyens, D. (2001) "Electrophysiological mechanisms of the long-QT syndrome in mice with targeted deletion of ^{1505}KPQ^{1507} in cardiac sodium channel." Program and abstracts of the North American Society of Pacing and Electrophysiology 22nd Annual Scientific Sessions; May 2-5; Boston, Massachusetts. Abstract 237.

92. Smith, M. R. and A. L. Goldin (1997). "Interaction between the sodium channel inactivation linker and domain III S4-S5." Biophys J **73**(4): 1885-95.